SANDIA REPORT SAND81—0998 • Unlimited Release • UC—32
Printed April 1984

JAC—A Two-Dimensional Finite Element Computer Program for the Non-Linear Quasistatic Response of Solids with the Conjugate Gradient Method

J. H. Biffle

Prepared by
Sandia National Laboratories
Albuquerque, New Mexico 87185 and Livermore, California 94550
for the United States Department of Energy
nder Contract DE-AC04-76DP00789

SF2900Q(8-81)

Issued by Sandia National Laboratories, operated for the United States Department of Energy by Sandia Corporation.

NOTICE: This report was prepared as an account of work sponsored by an agency of the United States Government. Neither the United States Government nor any agency thereof, nor any of their employees, nor any of their contractors, subcontractors, or their employees, makes any warranty, express or implied, or assumes any legal liability or responsibility for the accuracy, completeness, or usefulness of any information, apparatus, product, or process disclosed, or represents that its use would not infringe privately owned rights. Reference herein to any specific commercial product, process, or service by trade name, trademark, manufacturer, or otherwise, does not necessarily constitute or imply its endorsement, recommendation, or favoring by the United States Government, any agency thereof or any of their contractors or subcontractors. The views and opinions expressed herein do not necessarily state or reflect those of the United States Government, any agency thereof or any of their contractors or subcontractors.

Printed in the United States of America
Available from
National Technical Information Service
U.S. Department of Commerce
5285 Port Royal Road
Springfield, VA 22161

NTIS price codes
Printed copy: A05
Microfiche copy: A01

SAND81-0998

JAC - A TWO-DIMENSIONAL FINITE ELEMENT COMPUTER PROGRAM FOR THE NON-LINEAR QUASISTATIC RESPONSE OF SOLIDS WITH THE CONJUGATE GRADIENT METHOD

J. H. Biffle
Division 1521
Sandia National Laboratories
Albuquerque, New Mexico 87185

ABSTRACT

The nonlinear conjugate gradient procedure is employed in the computer program JAC to solve quasi-static nonlinear mechanics problems. A set of continuum equations is used that is very convenient for use with the conjugate gradient method and accurately describes nonlinear mechanics involving large rotation and strain. The method is exploited in a two-dimensional plane strain or axisymmetric setting while using various methods for accelerating convergence. Sliding interface conditions are also implemented. A four-node Lagrangian uniform strain element is used with orthogonal hourglass viscosity to control the zero energy modes. Materials which can be modeled include temperature dependent elastic-plastic, soils, and secondary creep behaviors. The program is vectorized to perform on the CRAY 1 computer.

Sample problems described are the bending of a thin beam, transverse crushing of a cylinder, extrusion of a plate and cylinder, bending of a laminated beam with interlaminear sliding and creeping of a cylinder.

ACKNOWLEDGMENT

The research for the work represented by this document could not have been accomplished without the support of S. W. Key and the contributions of the constitutive models by R. D. Krieg. I have also relied heavily on the advice of the staff of the Engineering Analysis Department who have used the JAC program. I am also grateful to N. J. Moore for her perseverance and understanding while preparing the manuscript.

Table of Contents

		Page
I.	INTRODUCTION	7
II.	THE EQUATIONS	9
	1.0 Continuum Equations	9
	2.0 Variational Statement	10
	3.0 Finite Element Equations	11
III.	ITERATIVE SOLUTION	13
IV.	TWO DIMENSIONAL APPLICATION	17
	1.0 Plane Strain Element	17
	2.0 Axisymmetric Element	19
	3.0 Sliding Interfaces	20
V.	MATERIAL PROPERTIES	22
	1.0 Isothermal Elastic-Plastic	22
	2.0 Temperature Dependent Elastic-Plastic	24
	3.0 Secondary Creep	25
	4.0 Soil and Crushable Foam	27
VI.	EXAMPLE PROBLEMS	29
	1.0 Large Displacement Beam	29
	2.0 Tube Crushing	29
	3.0 Extrusion	30
	4.0 Laminated Beams	31
	5.0 Creep Analysis of a Thick Walled Cylinder	31
VII.	REFERENCES	51
VIII.	USER INSTRUCTIONS	56
	1.0 Title Card	56
	2.0 Control	56
	3.0 Material Card Sets	63
	Material Type 1 - Isothermal Elastic-Plastic	63
	Material Type 2 - Temperature Dependent Elastic-Plastic	64
	Material Type 3 - Temperature Dependent Secondary Creep	65
	Material Type 4 - Isothermal Soil and Crushable Foam	67
	4.0 Function Cards	69
	5.0 Boundary Condition Cards	70
	6.0 Sliding Interface Condition Cards	71
	7.0 Convergence Control Card	72
IX.	JAC OUTPUT DESCRIPTION	73

I. INTRODUCTION

JAC is a finite element computer program for solving large deformation, temperature dependent quasi-static mechanics problems in two dimensions with the non-linear conjugate gradient (CG) technique. Either plane strain or axisymmetric geometry assumptions may be used with material descriptions which include temperature dependent elastic plastic, temperature dependent secondary creep and isothermal soil models. A four node Lagrangian uniform strain element is employed with orthogonal hourglass viscosity control of the zero energy modes.

Various schemes may be used to accelerate convergence of the CG method. One technique is to use as a starting vector some fraction of the velocity vector obtained from the previous load step. A second scheme is to first solve a load step while using a linear geometry approximation to the equations of motion. Then the linear geometry solution is used as a starting vector to solve the non-linear geometry problem.

For the calculation of the nonlinear quasi-static response of solids, there is a need for efficient and reliable solution methods. Obtaining finite element nonlinear solutions to static problems has represented a formidable task to engineers. The computer programs which are widely used, for example the ADINA code [1] and the MARC code [2], rely on the stiffness approach, using either a modified or unmodified Newton-Raphson method to solve the nonlinear problem. Use of the stiffness approach is troublesome because of the difficulty in deciding when to reformulate the stiffness matrix to keep the solution from diverging or to accelerate the convergence. On the opposite end of solution method types are explicit iterative methods which do not involve a stiffness matrix.

The impetus to try iterative solvers comes from several sources. First, there is a need to solve three-dimensional problems efficiently without restrictions on the number of elements which can be used because of hardware limitations in storing and retrieving the stiffness matrix from a magnetic disk. Secondly, a case can be made for explicit methods based on experiences with implicit versus explicit methods for dynamic problems. The explicit techniques appear to be more reliable in obtaining good solutions. Implicit techniques for solving nonlinear dynamic problems suffer from some of the same problems as are experienced by static algorithms that use the stiffness method. When it was realized that explicit solution to dynamic problems was effective, as implemented for example, in such codes as HONDO [3], WULFF [4], DYNA2D [5], DYNA3D [6] and SAMSON2 [7], then problems with the stiffness matrix could be circumvented. It can be argued that if an analyst knows his problem well enough to take large time steps and to make decisions about when to update the stiffness matrix and when to use equilibrium iterations, then a cheaper solution can be obtained using an implicit rather than an explicit technique. However, the analyst seldoms know enough about his problem in the beginning to arrive at an effective solution strategy. Based on this background in structural dynamics, it is now time to reexamine explicit techniques for use in solving nonlinear static problems.

In the early 1960's iterative techniques, such as successive overrelaxation, Gauss-Seidel, and Jacobi's methods were tried on finite element equations. It was soon discovered that direct solution procedures,

Gaussian elimination for example, were much more efficient than iterative techniques if the equations were numbered in an efficient manner. However, only linear or mildly nonlinear problems were being solved at that time. Rashid reopened the question of whether to use iterative techniques for three-dimensional problems and his technique is discussed by Irons [8]. With vector processing machines, it is very useful to use iterative techniques with their vectorization potential for two and three-dimensional problems because storage requirements and input-output operations will continue to limit the stiffness method. A reliable iterative method, even if expensive, is superior to a stiffness approach that does not reliably produce a solution on the first attempt.

After examining and trying various explicit techniques, the conjugate gradient (CG) technique [9,10,11] was selected for solving nonlinear solid mechanics problems. These nonlinear effects include material nonlinearities and geometric nonlinearities due to large rotations, large strains, and surfaces which slide relative to one another. The CG technique was selected mainly for its reliability. In particular, convergence for a linear problem is guaranteed with an infinite arithmetic machine in N steps where N is the number of unknowns in the problem. Also, various investigators in the field of linear programming and optimization are using the CG technique with some success [12,13,14]. Nonlinear versions of the CG technique are reported in reference [15] and [16]. Some acceleration techniques for the linear CG methods are discussed in reference [12].

In this document, a Lagrangian formulation of the mechanical equations is used in the current configuration of the body with particular attention being paid to the rotation of the stress tensor. The formulation is extremely amenable to the CG method because a stiffness matrix need not be calculated. Variational statements are then presented which allow a finite element representation of the equations of equilibrium.

II. THE EQUATIONS

1.0 Continuum Equations

To define the problem of large deformation static response, three sets of equations are needed. The first set consists of kinematic statements, the second of constitutive equations, and the third comprises the equations of equilibrium. The three sets of equations describe the process in the current configuration (deformed configuration) of the body at time t. Cartesian coordinates are used throughout the report. The current spatial position x of each material particle X in the body is given by the motion χ; thus

$$x = \chi(X,t) \tag{1}$$

The reference configuration is taken to be that of the body at t = 0. The equations are discussed in detail in reference [17].

The kinematic tensors which are of interest are the rate of deformation tensor D and the spin tensor W. The two tensors D and W can be written in terms of the velocity gradient tensor L as

$$D = (L+L^T)/2 \tag{2}$$

and

$$W = (L-L^T)/2. \tag{3}$$

Thus,

$$L = D + W \tag{4}$$

The components of L are

$$L_{km} = v_{k,m} \tag{5}$$

where the comma denotes partial differentiation and v is the velocity vector.

The kinematic boundary conditions are written as

$$v_i = \hat{v}_i \text{ on } s_1, \tag{6}$$

where s_1 is the portion of the surface on which velocity boundary conditions are specified.

Specific constitutive equations for different types of materials need not be discussed in detail here to develop the equations. It is only necessary to say that the constitutive equations can be written in the form

$$\dot{T}_{ij} = \mathcal{G}(L_{ij}, T_{ij}), \tag{7}$$

where the Cauchy stress tensor is T and $\mathcal{G}$ is a function of L_{ij} and T_{ij}. The stress boundary conditions are

$$t_i = \hat{t}_i \text{ on } s_2 \tag{8}$$

where $\hat{t}_i$ are the tractions prescribed over surfaces s_2 of the body.

In component form, the equations for static equilibrium of a body subject to prescribed body forces are

$$T_{ij,j} + \rho b_i = 0 \tag{9}$$

where ρ is the density and b_i is the body force per unit mass.

2.0 Variational Statement

In order to obtain finite element equations, a variational statement is needed. A more complete discussion of the variational problem in the context of dynamics is presented in [18]. The equations below follow [18] if the acceleration vector used in [18] is set equal to zero.

To obtain a variational principle for use with the finite element technique, the power input to the body (which is zero for the static problem) is written as

$$P_{input} = \int_S t_i v_i ds + \int_V \rho b_i v_i dV , \tag{10}$$

where s denotes the surface and V the volume of the body in the deformed configuration. Since $t_i = T_{ij} \cdot n_j$ on s_2, where the quantities n_j are the components of the unit normal to the surface, the surface integral in (10) can be transformed into

$$P_{input} = \int_V \left[v_i \ (T_{ji,j} + \rho b_i) + T_{ji} v_{i,j} \right] dV. \tag{11}$$

A functional π is now defined by the equation

$$\pi = \int_V \left[v_i T_{ji,j} + T_{ji} v_{i,j} \right] dV - \int_S t_i v_i ds = 0. \tag{12}$$

If the equilibrium equations are substituted for $T_{ji,j}$ in (12), the second term integrated by parts and the first variations taken, the result is

$$\delta\pi = \int_V \delta v_i (-\rho b_i - T_{ji,j}) dV - \int_{S_2} \delta v_i (\hat{t}_i - t_i) ds. \tag{13}$$

The Euler equations are the traction boundary conditions (8) and the equilibrium equations (9). If, in equation (13), the term involving $T_{ji,i}$ is integrated by parts, the following first variation is obtained

$$\delta\pi' = \int_V \delta v_i \ (-\rho b_i) dV + \int_V \delta v_{i,j} T_{ij} dV - \int_{S_2} \delta v_i t_i ds = 0. \tag{14}$$

In the finite element method, equation (14) will be used to determine the residual forces in the body at each iteration to obtain a final solution.

3.0 Finite Element Equations

To obtain finite element equations for (14), it is assumed that the velocities are approximated by a set of continuous functions with undetermined coefficients. Matrices of interpolation functions, ϕ, are used for vector quantities. In the following equations, all quantities are composed of tensor or vector components in vector or matrix form.

The equations (1) through (14) describe a quasi-static theory in which velocities are retained but the time rates of velocities are neglected. Some quasi-static mechanical processes involve real times such as those involving viscoelastic and creeping materials. Others, for example, involving elastic or elastic-plastic materials, proceed independently of the amount of time used in the process. The present analysis will be described in terms of real time. When going from time t_{n-1} to t_n, an interval of time, Δt, is used

$$\Delta t = t_n - t_{n-1} \tag{15}$$

where n is called the time step (load step) number. In order to be consistent, time will always be used as a load stepping device. The index j is used to refer to an iteration within a load step.

Given the velocity gradients (5), which is rewritten here in vector form as

$$L_j = \nabla\phi \; v_j \; , \tag{16}$$

the constitutive relationship is evaluated as

$$T_j = Q_j^T \; Q_j \; T_{n-1} Q_j + \quad Q_j^T \; T_{n-1} Q_j \, , \; D_j \; \Delta t \; Q_j \, , \tag{17}$$

where

$$Q_j = f(W_j)\Delta t \, . \tag{18}$$

The quantity T_j is a vector of components of the stress tensor and Q_j is a matrix describing the rotation of the material at the point in question. Hallquist [19] and Hughes [20] have shown that, if the velocity gradients are evaluated at the midstep, the resulting strain is invariant to rigid body rotation. Also, the resulting integrated incremental strain closely approximates the true strain for large extensions. The operation with the matrix Q_j represents one-half the rotation that occurs between time t_{n-1} and t_n. In equation (17), the stress at time t_{n-1}, is rotated to the midstep, and then used in the constitutive function. The resulting stress is then rotated to the end of the step. This large rotation theory has a defect in that the shear stress exhibits an oscillatory behavior under large shear straining. There are several theories [21], [22] and [23] under discussion for use in correcting the problem, however at this time the technical community has not reached general agreement on the best approach. The present theory is satisfactory up to approximately a shear strain of 1.0. JAC should be used with caution for large shear strains.

The finite element equations that represent the variational statement (14) are

$$R_j = \sum_{e=1}^{N} \left[\int_{V_e(x_i)} (\nabla\phi)^T T_j dV - \int_{V_e(x_i)} \phi^T \rho b_n dV - \int_{S_e(x_j)} \phi^T \hat{t}_n ds, \right] \tag{19}$$

where the integrations are performed with the body in the configuration currently predicted for the end of the time step. In general, the residual force vector R_j will not be exactly zero as required for equilibrium. The objective of the iteration procedure is to reduce the residual forces to an acceptably low value.

III. ITERATIVE SOLUTION

The following equations describe the nonlinear conjugate gradient iterative procedure for using equations (16)–(19) to calculate a residual force vector R_j. A generalized procedure described in [11] is used, where Z_j is the generalized residual vector. For each iterate j,

$$Z_j = M_n^{-1} R_j \tag{20}$$

where M_n is a weighting matrix. The weighting matrix is usually taken as the diagonal terms of the stiffness matrix, although other forms have been considered [11]. The conjugate gradient vector P is calculated using

$$P_{j+1} = Z_j + \beta_j P_j \tag{21}$$

where

$$\beta_j = \begin{cases} \dfrac{Z_j^T M_n Z_j + Z_{j-1}^T M_n Z_j}{Z_{j-1}^T M_n Z_{j-1}} & , j \neq 0. \\ 0. & , j = 0. \end{cases} \tag{22}$$

Then the velocity estimate is updated using

$$v_{j+1} = v_j + \alpha_j P_{j+1}, \tag{23}$$

where α_j is determined such that

$$P_{j+1}^T R(v_{j+1}) = 0. \tag{24}$$

The displacements and positions of the material particles are then updated using the formula

$$u_{j+1} = u_{n-1} + v_{j+1} \Delta t \tag{25}$$

$$x_{j+1} = x_{n-1} + v_{j+1} \Delta t \tag{26}$$

The conjugate gradient process starts at the beginning of each load step by assuming a velocity vector, v_o, and using equation (16) for the velocity gradient vector. Then the constitutive equations at each node are solved using equations (17) and (18). The residual force vector is calculated with equation (19) which in general will not be equal to zero. In order to reduce the residual force, a conjugate gradient vector is calculated using (20), (21), and (22). If the process were linear, then the second term in the numerator of equation (22) would be zero since Z_j would be orthogonal to Z_{j-1}. This form for β_j comes from reference [14] and the generalized residual vector given by equation (20) from reference [11]. Both the weighting matrix and the second term in (22) for β can be considered as convergence acceleration devices.

Equation (24) to find α_j presents a few problems. Since the solution to nonlinear structural problems is wanted, then equation (25) is nonlinear in α_j as seen when $v_j + \alpha_j P_{j+1}$, is substituted into (16) - (19). The value of α_j is usually found with an expensive line search using, for example, a Newton-Raphson method in solving equation (24). However, it is difficult to calculate the derivative of R with respect to α_j. Instead of a line search, a technique which will usually work for mechanics problems is to require that the constitutive model provide a secant modulus, C_s, for use in the following calculations, equations (27)-(30). If a secant modulus is not available, the elastic constitutive matrix may be used but convergence will be slower.

$$L_{P_{j+1}} = \nabla\phi \; P_{j+1} . \tag{27}$$

$$T_{P_{j+1}} = C_{s_j} \; D_{P_{j+1}} . \tag{28}$$

$$R_{P_{j+1}} = \sum_{e=1}^{N} \int_{V_e(x_j)} (\nabla\phi)^T \; T_{P_{j+1}} \; dV . \tag{29}$$

$$\alpha_j = \frac{Z_j^T \; M_n \; Z_j}{P_{j+1}^T \; R_{P_{j+1}}} \tag{30}$$

The iteration process continues by incrementing j and solving equation (16) again.

Velocity boundary conditions are imposed by setting the values in the initial velocity vector, v_o, to the values needed to obtain the prescribed displacements and then the corresponding components of R_j are set to zero. Stress boundary conditions and body forces are imposed in equation (19) using b_n and $\hat{t}_j$.

When the jth iteration loop satisfies a convergence criterion after calculation of equation (19), the stresses, coordinates, and displacements for use at the beginning of the next load increment are updated. This is written as

$$T_n = T_j \tag{31}$$

$$x_n = x_j \tag{32}$$

and

$$u_n = u_j \tag{33}$$

Convergence at a time step is defined to have taken place when either of the following inequalities is satisfied,

$$\left(\frac{||\Delta u_{j+1}|| - ||\Delta u_j||}{||\Delta u_{j+1}||} \right)^{1/2} \leq \text{TOLU}. \tag{34}$$

or

$$\left(\frac{||R_j||}{||F_n||} \right)^{1/2} \leq \text{TOLR}. \tag{35}$$

$||A||$ represents the L^2 norm of a vector. In equation (35), F_n is a vector containing the applied tractions, body forces, gravity loads, thermal loads, and reactions at nodes where nonzero displacement boundary conditions are applied. It is important to satisfy equilibrium conditions at the end of each time step so that the value of the equilibrium convergence criteria equation (35) should be reached first. The incremental displacement condition, equation (34) should be used to stop a nonconverging solution. The program will terminate execution if either equation (34) or (35) is satisfied. The default tolerances for equations (34) and (35) are 1.0×10^{-6} and 0.001, respectively.

The matrix M_n is used to accelerate the conjugate gradient convergence process. It is taken to be a diagonal matrix with values equal to the diagonal of the stiffness matrix with linear elastic properties used. It is calculated only once, at the beginning of each time step (load step), and held constant during the iterative process. This choice of M_n is particularly useful in axisymmetric problems or when different parts of the body contain different elastic properties.

Another way to accelerate the convergence is to provide a good starting velocity vector. It is very helpful if the starting vector contains information about the lowest mode shapes which may be present in the solution. In many cases, a good starting vector is some fraction of the velocity calculated for the previous time step. This is particularly true if the directions of the imposed tractions are not significantly changed between steps. Another convergence acceleration technique is to first obtain a solution for the velocity with linear geometrical assumptions. Then the linear solution is used as a starting vector to calculate the geometrically nonlinear solution. This technique appears to be most useful when the solution is dominated by geometric nonlinearities. Excluding geometrical effects is easily accomplished by not updating the coordinates x_j for the integrations and by not rotating the stress vector.

The program has an element birth and death option which allows a block of elements with the same material identification number to be active for solution times which are between a specified birth time and a death time. If the solution time is outside the active time range, the elements are simply skipped in the residual force and conjugate gradient parameter calculations.

The JAC computer program is vectorized to perform efficiently on the CRAY 1 computer. The vectorization method is called block vectorization and is described in reference [24]. In general within a group of elements using the same material identification number, the elements are processed in blocks of up to 128. The residual force vector is obtained by processing equations (16) - (19) for each block of elements. The calculation of the α_j conjugate parameter in equations (27)-(30)is also vectorized using this block vectorization method.

IV. TWO-DIMENSIONAL APPLICATION

The computer program JAC uses a two-dimensional application of the CG iteration technique. Devices to accelerate convergence of the solution as well as sliding surface constraints are implemented. All the ideas used can be readily extended to three-dimensional geometry.

1.0 Plane Strain Element

For the two-dimensional application, four-node isoparametric elements are used. The four node uniform strain element quadrilateral with orthogonal hourglass control which is used for plain strain calculations is described in reference [25] by Flanagan and Belytschko. The results are reviewed here and then an extension to the axisymmetric element by Flanagan [26] is discussed. The element is derived by first writing the interpolation functions in terms of an orthogonal set of physical base vectors as

$$4\,\phi_I = \Sigma_I + \xi\Lambda_{1I} + \eta\Lambda_{2I} + \xi\eta\Gamma_I \tag{36}$$

where Table 1 describes the base vectors.

Table 1

Node, I	ξ	η	Σ_I	Λ_{1I}	Λ_{2I}	Γ_I
1	−1	−1	1	−1	−1	1
2	1	−1	1	1	−1	−1
3	1	1	1	1	1	1
4	−1	1	1	−1	1	−1

The isoparametric coordinates ξ and η have a range of −1 to +1.

The uniform velocity gradient operator components for equation (16) are defined as

$$\bar{v}_{i,j} = \frac{1}{V_e}\, v_{iI} \int_{V_e} \phi_{I,j}\, dV \tag{37}$$

where the bar ($^-$) denotes a uniform quantity. Assuming a unit thickness for the plane strain element, the volume V_e is then calculated by

$$V_e = x_I\, y_J \int_{-1}^{1}\int_{-1}^{1} (\phi_{I,\xi}\,\phi_{J,\eta} - \phi_{I,\eta}\,\phi_{J,\xi})\, d\eta\, d\xi \tag{38}$$

These results are the same as with a single point integration when using the center of the element. The difference in the customary single point element and the uniform strain element is in the representation of the hourglass forces. The hourglass forces are found by first expressing the linear part of the velocity field as

$$v_i^{LIN} = \bar{v}_i + \bar{v}_{i,j} (x_j - \bar{x}_j). \tag{39}$$

The hourglass field v_{iI}^{HG} is now defined by removing the linear portion of the nodal velocity field:

$$v_{iI}^{HG} = v_{iI} - v_{iI}^{LIN} \tag{40}$$

In [25] it is shown the v_{iI}^{HG} is orthogonal to all of the base vectors in Table 1 except the Γ_I vector. Therefore, the hourglass field can be expanded as a linear combination of the Γ_I vectors as:

$$v_{iI}^{HG} = q_{i\alpha}\Gamma_{\alpha I} \ . \tag{41}$$

where $q_{i\alpha}$ represents the hourglass velocities. By defining the hourglass velocities $q_{i\alpha}$ as

$$q_{i\alpha} = \frac{1}{2} v_{iI} \gamma_{\alpha I}, \tag{42}$$

it is shown in [25] that the hourglass shape functions γ are

$$\gamma_I = {}_I - \frac{1}{V_e} x_{iJ} \Gamma_J \int_{V_e} \phi_{I,i} dV \tag{43}$$

The antihourglass forces are computed by

$$f_{iI}^{HG} = \kappa \gamma_J \gamma_J v_{iI} \tag{44}$$

where

$$\kappa = \varepsilon \frac{C_{44}}{V_e} \int_{V_e} \phi_{iI} dV \int_{V_e} \phi_{iI} dV \ . \tag{45}$$

In contrast to [25] where elastic hourglass control is discussed, the use of the secant shear modulus, C_{44} is necessary to account for reductions in

element stiffness due to plastic straining when using a elastic-plastic material model. The secant shear modulus is defined in the material properties section of this document. The best value for the constant ε was experimentally determined from a series of numerical analyses to be 1/30.

2.0 Axisymmetric Element

For the axisymmetric element [26], the element volume is written, where r is the radial component, as

$$V_e = r_I r_J r_K \int_{-1}^{1}\int_{-1}^{1} \phi_I \; (\phi_{J,\xi}\phi_{K,\eta} - \phi_{J,\eta}\phi_{K,\xi}) d\eta d\xi \tag{46}$$

which can be analytically integrated. The uniform velocity gradient components are

$$\bar{v}_{i,j} = \frac{1}{V_e} \; v_{iI} \int_{A_e} \phi_{I,j} dA \tag{47}$$

and

$$\frac{\bar{v}_r}{r} = \frac{1}{V_e} \; v_{rI} \int_{A_e} \phi_I \; dA \tag{48}$$

The above definitions yield the important identity

$$\dot{V}_e = \bar{v}_{i,i} + \frac{\bar{v}_r}{r} \tag{49}$$

so that the correct volume change is calculated when using the uniform velocity gradient components.

Using a derivation as in [25] for the plane strain element, the hourglass shape functions for the axisymmetric element [26] can be shown to be

$$\gamma_I = \Gamma_I - \frac{1}{V_e} \; r_{iJ} \; \Gamma_J \int_{A_e} \phi_{I,i} dA \tag{50}$$

In two dimensions, the spin tensor W in equation (3) has only one non-trivial component:

$$\bar{W}_{xy} = 1/2(\bar{v}_{x,y} - \bar{v}_{y,x}) \tag{51}$$

The angle which is used in the definition of the matrix Q is given by

$$\theta = \tan^{-1} (1/2\ \bar{W}_{xy} \Delta t) \quad . \tag{52}$$

3.0 Sliding Interfaces

Many structures consist of two or more parts which are in contact and slide with respect to one another. In the context of the CG method, a sliding algorithm can easily be incorporated using the master-slave concept. When interference between two surfaces is detected, the nodes on the slave surface are constrained to move in a direction normal to the master surface. Friction can be used to constrain differential motion of the two surfaces in the direction tangent to the master surface. The relationship between a slave node and a master surface is shown in Figure 1. The slave node if unimpeded would move to point 3 in Figure 1.

If $|d|$ in Figure 1 is larger than some previously specified value and the normal force F_n is also larger than a previously specified value, then penetration of a slave node into the master surface is defined as having occurred.

The residual forces present at slave node 3 rotated to the n-s coordinate directions are calculated as

$$\begin{bmatrix} R_{3n} \\ R_{3s} \end{bmatrix} = U \begin{bmatrix} R_{3x} \\ R_{3y} \end{bmatrix} \tag{53}$$

where U is a rotation matrix which defines the n-s coordinate system with respect to the x-y system. The normal force R_{3n} is applied to the master surface at 4 but the amount of force to be applied in the tangential direction is dependent upon the coefficient of friction. If μ is the coefficient of friction, then the tangential force F_s is the minimum of the friction force μR_{3n} and the residual, R_{3s}. The positive direction of F_s is the same as that of R_{3s}. The forces R_4 to be applied at the master surface location 4 are

$$\begin{bmatrix} R_{4x} \\ R_{4y} \end{bmatrix} = U^{-1} \begin{bmatrix} R_{3n} \\ F_s \end{bmatrix} \tag{54}$$

Point 4 is generally not a nodal location on the master surface and hence the force R_4 must be distributed to the master element nodes. The equation used to apply R_4 to the master surface is

$$R_i' = R_i + \phi_i R_4 \qquad i = 1,2 \tag{55}$$

where i is a master node number and ϕ_i are interpolation functions, evaluated at 4 .

The forces R_4 are then subtracted from the slave node residuals.

$$R_4'' = R_4 - R_4' \tag{56}$$

The conjugate gradient vector of the slave node must be modified so that the velocity of the slave node will eventually be the same as the velocity of the master surface at 4 . First, P_3 , the conjugate gradient vector of the slave node, is rotated to the n-s coordinate system.

$$\begin{bmatrix} P_{3n} \\ P_{3s} \end{bmatrix} = U \begin{bmatrix} P_3 \\ P_{3y} \end{bmatrix} \tag{57}$$

Then the conjugate gradient vector of the master surface at point 4 is calculated with the interpolation functions by using the equation:

$$P_4^m = \phi_i P_i^m \tag{58}$$

Then P_4^m is rotated to the n-s coordinate system and the slave node conjugate gradient is now calculated using P_{4n}^m, P_{3s} and d:

$$\begin{bmatrix} P_{3x}^s \\ P_{3y}^s \end{bmatrix} = U^T \begin{bmatrix} P_{4n}^m - \dfrac{0.2|d|}{\alpha_j \Delta t} \\ P_{3s} \end{bmatrix} \tag{59}$$

When P_{3x}^s and P_{3y}^s are used in equation (23), the slave node will follow the master surface in the normal direction. In order to correct for the initial penetration distance, the factor $0.2|d|/\alpha_j \Delta t$ is used to reduce the distance on each succeeding iteration where α_j is the conjugate gradient parameter in equation (23).

The sliding algorithm can be simply changed to a fixed interface algorithm by applying all the residual slave forces to the master surface at 4 and then subtracting the slave residuals. The slave node is given the same slave node conjugate gradient vector as the master surface has at point 4 by using the value in (58).

V. MATERIAL PROPERTIES

The program is written in modular form so that different material models can be added in the future. At the present time, the code contains an isothermal elastic-plastic model, a temperature dependent elastic-plastic model, a temperature dependent elastic-secondary creep model, and a soil and crushable foam model.

The function $\mathcal{G}$ in equation (17) represents the constitutive relationship. The main approximation in the following models is that the strain rate is constant over the interval from time t_{n-1} to t_n.

1.0 Isothermal Elastic Plastic Model

The elastic-plastic linear strain hardening model is a combined isotropic-kinematic hardening model with a hardening parameter $0 \leq \beta \leq 1$ to specify the ratio of kinematic to isotropic hardening. A von Mises yield surface is used together with an associated flow rule. This method, used for the isothermal elastic-plastic calculations, is reported by Krieg and Key [27,28]. The behavior described by the model is shown in Figure 2 for uniaxial stress.

The numerical method for solving the resulting equations may be considered that of stepping out elastically in deviatoric stress space and, if the resulting "trial state" is beyond the yield surface, then scaling the stress radially back to the updated von Mises yield surface. The updated stress and the yield surface position and size are found simultaneously. The assumption of a constant strainrate over a time step used in the material subroutines is consistent since time rates of change of velocities are ignored in the program. The stress and plastic state update applies equally well for any general initial state at the beginning of the time step and for any strain increment size or direction. While a conceptually "simplistic" process, it is an excellent numerical approximation for integrating this rather conventional plasticity model. The accuracy of this "radial return" method has been compared by Krieg and Krieg [29] to other methods for the case of no hardening.

The details of the process are as follows. The stress is denoted as T_{n-1}, position of the center of the yield surface γ_{n-1}, and effective plastic strain $D_{p_{n-1}}$, and the strain rate $D_{n-1/2}$. The steps taken are:

(1) The radius σ_{y_j} of the yield surface is calculated using the equation

$$\sigma_{y_j} = T_{y_{n-1}} + \beta H D_{p_{n-1}} , \tag{60}$$

where

$$H = \frac{EE_t}{E-E_t} , \tag{61}$$

where the elastic modulus E, the plastic tangent modulus E_t, the yield stress T_y, and the hardening parameter β are material parameters identified in Figure 2. The elastic shear modulus G and the bulk modulus K are used in the following steps,

(2) The "trial" stress state T_j^T, the jth iteration approximation for the end of the increment, is calculated using a matrix of elastic constants C.

$$T_j^T = T_{n-1} + C\ D_j \Delta t \tag{62}$$

where T_{n-1} is the rotated stress indicated in equation (17).

(3) The trial deviatoric effective stress, S_j, is calculated,

$$S_j = \left[T_j^T - \gamma_{n-1} \right]_{deviator} \tag{63}$$

and its vector magnitude is compared to the radius of the yield surface:

$$\Phi = \sqrt{\frac{2}{3}}\ \left| S_j \right| - \sigma_{y_j} . \tag{64}$$

(4) The incremental process is elastic if $\Phi \leq 0$ and, in this case, the final stress is the trial stress:

$$T_j = T_j^T . \tag{65}$$

The incremental process is at least partially plastic if $\Phi \leq 0$ and the remaining step (5) must be executed.

(5) The updated value of the yield surface position and size (indirectly as the effective plastic strain) are calculated and the trial stress is scaled back to this surface to give the final stress.

$$C_5 = \frac{1 - \dfrac{\sqrt{2}/3\ \sigma_{y_j}}{\left| S_j \right|}}{1 + H/3\ G} \tag{66}$$

$$D_{p_j} = D_{p_{n-1}} + C_5 \left|S_j\right| / \sqrt{6} \quad G \tag{67}$$

$$\gamma_j = \gamma_{n-1} + (1-\beta) \frac{C_5 H}{3G} \quad S_j \tag{68}$$

$$T_j = T_j^{\,T} - C_5 \; S_j \tag{69}$$

The secant modulus used in the determination of the conjugate parameter α_j is calculated using the relations:

$$C_{pq} = 1/2 \; a_1 + K - a_2 \; S_p \; S_q \qquad p,\; q = 1,3 \tag{70}$$

$$C_{pp} = 2/3 \; a_1 + K - a_2 \; S_p \; S_p \quad \text{(no summation)} \; p = 1,3 \tag{71}$$

$$C_{4p} = C_{p4} = a_2 \; S_4 \; S_p \qquad p = 1,3 \tag{72}$$

$$a_1 = 2G(1-C_5) \tag{74}$$

$$a_2 = \frac{2G \sqrt{2/3} \; \sigma_{y_j}}{(1 + H/3G)\left|S\right|^3} \tag{75}$$

2.0 Temperature Dependent Elastic-Plastic Model

The temperature dependent elastic plastic model uses the radial return method as does the previously described elastic plastic model. The material properties; Young's modulus, Poisson's ratio, yield stress and hardening modulus, are assumed to vary linearly with temperature between the beginning and the end of the time step. First, the initial stress is adjusted to reflect the change in moduli due to temperature, then the trial stress is calculated. Instead of using the plastic strain as in (60) and (67) for the isothermal model, an updated value on the yield surface is calculated. Given the previous value of the yield radius $T_{y_{n-1}}$, and the initial yield radius values, T_{y_1} and T_{y_2}, at temperatures θ_{n-1} and θ_n, respectively, the radius of the yield surface is calculated by

$$\sigma_{y_i} = T_{y_{n-1}} + (T_{y_2} - T_{y_1}) + \frac{H_2 - H_1}{H_1} \; (\sigma_{y_{n-1}} - T_{y_1}), \text{ if } \beta \neq 0. \tag{76}$$

$$\sigma_{y_i} = T_{y_{n-1}} + T_{y_2} - T_{y_1}, \text{ if } \beta = 0. \tag{77}$$

The calculation of the stress state continues as with the isothermal model using average values of G and H. Instead of using equation (67), the yield surface is updated by

$$\sigma_{y_n} = \sigma_{y_j} + \frac{\beta H C_5 \left| S_j \right|}{\sqrt{6}\ G} \tag{78}$$

The secant modulus constants are calculated by using equations (70)-(75) with average material properties.

3.0 Secondary Creep Model

Secondary creep described by a power law form is used for the material model and is integrated in time by a technique described by Krieg in [24]. The effective creep strain rate, D_c for the material is represented by the scalar equation:

$$D_c = A_1\ \sigma_c^{A_2}\ e^{-A_3/\theta} \tag{79}$$

where A_1, A_2, and A_3 are material constants, θ is the absolute temperature, and σ_c is the effective stress.

The dilitational response is elastic. Tensor equations are used for the stress rate as a function of initial stress state and the imposed strain rate. The resulting mathematically stiff equations cannot be efficiently and accurately solved using ordinary numerical integration methods. Three separate regions are used and approximate but tractable tensor differential equations are derived for each. The analytical solutions of these approximate equations are then used to define a numerical method with acceptable accuracy and speed. The method has automatic internal multistepping based on accuracy limitations. For the five percent tolerance which is used, never more than eight multisteps are needed and usually only one step is used.

Equation (79) is used to derive a tensor valued differential equation for the deviatoric stretching tensor S as

$$\dot{S}_j = a_j - b S_j^{A_2} \tag{80}$$

where

$$a_j = 2G\ D_j \tag{81}$$

$$b = 2G(1.5)^{0.5(A_2+1)}\ A_1 \tag{82}$$

G is the average elastic shear modulus over the temprature span during the time step.

The three regions for which (80) is approximated are:

(1) The case when $b|S_j|^{A_2} << |a_j|$ where an expansion about the initial stress state is used since the response is nearly elastic. the resulting equations are

$$S_j = S_{n-1} + \left\{A_2 a_j - \left[(A_2-1)\rho + \beta\right] S_{n-1}\right\} \left(\frac{1-e^{-\beta t}}{A_2\beta}\right)$$

$$- \left(\frac{\rho - \beta}{A_2\beta}\right) S_{n-1} \left(e^{-A_2\beta t} - e^{-\beta t}\right) \tag{83}$$

where

$$\beta = b|S_\infty|^{A_2-1} \tag{84}$$

$$S_\infty = \frac{|a_j|^{\frac{1-A_2}{A_2}}}{b}\ a_j \tag{85}$$

$$\rho = \frac{S_{n-1} \cdot a_j}{S_{n-1} \cdot S_{n-1}} \tag{86}$$

$$C_o = b|S_{n-1}|^{A_2-1} \tag{87}$$

(2) The second case is when $b|S_j|^{A_2} \cong |a_j|$ where an asymptotic solution is obtained in the neighborhood of S_∞. The resulting equations are

$$S_j = S_\infty - (S_{n-1} - S_\infty)e^{-\beta t} + \left(\frac{S_{n-1}}{S_\infty} \cdot \frac{S_\infty}{S_\infty} - 1\right) S_\infty \left(e^{-A_2\beta t} - e^{-\beta t}\right) \tag{88}$$

(3) The third region is when $|a_j| << b|S_j|^{A_2}$ and the elastic terms can be neglected. The resulting solution is

$$S_j = \frac{a_j}{A_2 C_o}\left[1-(A_2-1)C_o t\right] + \frac{S_{n-1} - A_j/A_2 C_o}{\left[1+(A_2-1)C_o t\right]^{1/(A_2-1)}} \tag{89}$$

The accuracy is controlled by using appropriate time sub-increments within each case and defining the boundaries between cases. The present version of the model is accurate for $A_2 = 5$. Care should be used for a value of A_2 for from 5.

With the creep model, an elastic modulus instead of a secant modulus is used in equation (29) for determination of the conjugate gradient parameter.

4.0 Soil and Crushable Foam Model

Soils and crushable foams exhibit a behavior that is pressure dependent. Because of voids, they crush or compact under pressure. Their failure in shear can also be sensitive to pressure. Krieg [30] models these characteristics using an isotropic pressure dependent deviatoric plasticity theory and an arbitrary volumetric plasticity. The yield surface in principal stress space is a surface of revolution centered about the hydrostat with the open end pointing into compression. The open end is capped with a plane which is at right angles to the hydrostat. The deviatoric part is elastic-perfectly plastic so the surface of revolution is stationary. The volumetric part has variable strain hardening so the end plane moves outward during volumetric yielding. A flow rule is used such that deviatoric strains produce no volume change. The material is assumed to be intact, i.e., tensile fracture has not occurred so long as the pressure, P is greater than h, where h is the minimum root of the polynomial $A_1 + A_2P + A_3P^2 = 0$. If fracture occurs, the pressure is set equal to h.

The function f which describes the pressure versus the volume strain behavior is depicted in Figure 3. Unloading from any point along the curve is taken to be elastic with a modulus of K_0.

The steps taken are as follows:

(1) The pressure p and the deviatoric stress S at time n are computed. The volumetric strain rate D_v and deviatoric strain rate D_s at $t_{n-1/2}$ are computed.

(2) The volumetric strain at t_n is calculated and compared to the past minimum E_{v_m}.

$$E_{v_j} = E_{v_{n-1}} + D_{v_{n-1/2}}\Delta t \tag{90}$$

If $E_{v_j} > E_{v_m}$, the step is elastic and

$$P_j = P_{n-1} - K_o D_{v_{n-1/2}} \Delta t \tag{91}$$

If $E_{v_j} \leq E_{v_m}$, plastic loading is occuring and

$$P_j = f(E_{v_j}) \tag{92}$$

$$E_{v_m} = E_{v_j} \tag{93}$$

after the step has converged.

(3) A check for tensile failure is made. If failure has occurred, the pressure at t_n is set equal to h. The stress state is then at the tip of the surface of revolution and the deviatoric stress must be zero

$$T_j = P_j = -h \tag{94}$$

If failure has not occurred, the deviatoric stresses are sought.

(4) The deviatoric components of the stress are calculated as in the elastic-plastic models with the radial return method. In this case the hardening modulus E_t and the hardening parameter β are zero.

With the soil model, a secant modulus is calculated by employing equations (70)-(75).

VI. EXAMPLE PROBLEMS

Example problems are included for use in code verification and to acquaint the user with the input and types of problems which can be calculated. The problems include the large displacement bending of a beam, transverse crushing of a cylinder, extrusion of a plate and cylinder, bending of a laminated beam with interlamination sliding, and creeping of a cylinder.

1.0 Large Displacement Beam

The large deformation of an elastic cantilever beam is included since an analytical solution by Holden [31] is available. It also demonstrates a problem with which the CG method has great difficulty. The beam has a length to thickness ratio of 30 and Poisson's ratio is set equal to zero. Two solutions are reported. The beam is loaded with a uniformly distributed vertical load and with a pressure normal to the surface. Thirty elements are used along the length and four through the thickness.

Shown in Figure 4 is a comparison of the analytical results both with and without non-linear terms as reported in [31], and the numerical results due to a gravity load, i.e., one in which the forces in the beam are in the vertical direction. The comparison is very good. For the gravity loading, the value of P in the figure is gravity load divided by the length of the beam. Also shown in the figure are the numerical results for a pressure loaded beam where the forces are always normal to the beam. Figure 5 depicts the actual deformed shape of the beam due to gravity loading at $k = 6.48$.

Convergence of the solution for the beam problem is very slow. First, the spread of eigenvalues in the problem is large and any explicit interative technique will have difficulties. If the problem is ill-conditioned in the linear approximation, as in this case, then adding the nonlinearity of large deformation, i.e., taking into account the rotation of the beam, compounds the difficulty. To ease the difficulties of the non-linearities, the calculation is begun by first solving the linear problem. Then, using the linear result as a starting vector, the geometric nonlinear effects are included. The starting vector for each time step is taken to be the velocity of the previous step. After the first load step, each step took approximately 220 linear iterations followed by approximately 310 nonlinear iterations. Load increments of $k = 0.0328$ for the pressure loading and load increments of $k = 0.0628$ were used for the gravity loading. A convergence tolerance of 0.03 for the force norm of equation (35) was used.

2.0 Tube Crushing

The plane strain crushing of a relatively thin tube in the diametrical direction by rigid platens represents a difficult elastic-plastic, large deformation and sliding surface problem for a finite element technique. The geometry and material properties of the problem are shown in Figure 6. The surface between the tube and the platen is assumed to be frictionless. Shown in Figure 7 is the finite element model.

A displacement is applied to the tube at the lower symmetry plane. Displacement control is needed because the load-deflection response is soft after plastic hinges have formed at the top and bottom of the ring quadrant. Four elements are needed through the thickness in order to accurately represent a plastic hinge stress state through the thickness. The displacement of 2.921 x 10-4 m was applied in 10 steps, followed by 20 steps to 0.00254 m of total displacement, then equal steps of 2.75 x 10-4 m. The deformed shape at a deflection of 0.01778 m is shown in Figure 8. The results are shown in Figure 9 for the total load on one platen versus the displacement δ , where r is the initial midsurface radius.

The results are compared to both analytical [32] and experimental results [33]. The applied load is normalized to the load that will cause plastic hinges to first appear, which is

$$P_o = \frac{2\sigma_y h^2}{\sqrt{3}} \tag{95}$$

The solution strategy consisted of obtaining a linear geometry solution followed by a geometrically nonlinear solution. It took approximately 1300 iterations for the linear geometry solution and 300 iterations for nonlinear geometry solutions to achieve convergence for each step. A force convergence tolerance of 0.001 was necessary to obtain a satisfactory load deflection curve.

3.0 Extrusion

The problem of the plane strain extrusion of a plate [32] is included to demonstrate a case where large amounts of sliding take place, along with elastic-plastic loading and unloading. The geometry, properties for the elastic-perfectly plastic material and and initial finite element mesh are shown in Figure 10. The sliding surface is assumed to be frictionless. A displacement is applied to the left end to move the material. The deformed mesh plot at the applied displacement of 0.0381 m is shown in Figure 11.

The applied load is plotted as a function of the applied displacement in Figure 12. The ragged appearance of the plot is due to the small number of elements used to describe the pressure along the interface. The solution strategy was the same as was used for the crushed tube problem. It took approximately 1000 and 500 iterations, respectively, for convergence of the linear and the nonlinear geometry solutions for each displacement load step. Seven load steps of 0.00254 m were followed by steps of 0.00177 m. A force norm convergence tolerance of 0.001 was used.

The extrusion problem was also calculated using the axisymmetric element. The results were similar to the plane strain calculations. The deformed mesh at a displacement of 0.0356 m is shown in Figure 13 and the load deflection curve is shown in Figure 14.

4.0 Laminated Beams

A laminated beam problem is used to demonstrate the behavior of multiple sets of slide lines. The problem is a simulation of the reaction of layers of material above an underground mine opening. An experiment was performed which is described in [35]. A centrifuge was used to simulate enhanced gravity loads and a lamination of foundry stone was made up of 0.0254 m thick beams, 0.267 m long. The geometry of the experiment is shown in Figure 15, along with the material properties and loading sequence. The coefficient of friction between layers was experimentally found to be approximately 0.50. Sliding interfaces were used between the beams and separation of the beams was allowed to preclude development of tensional stress normal to the interfaces.

The finite element model which was used is shown in Figure 16 where symmetry is used.

In the experiment, the rotational speed of the centrifuge was increased until all the beams above the opening were cracked. This occurred at a load of 150.3 g's. The ultimate tensile strength of the material is approximately 917 kPa while the computer code predicted 830 kPa at 150.3 g's at point A in Figure 19, at the center of the opening. Figure 15 shows the deformed shape at 150.3 g's magnified 200 times to show the sliding.

The solution strategy adopted consisted of obtaining a geometrically linear solution followed by a geometrically nonlinear solution for each load step. It took approximately 1000 iterations for the linear solution followed by one iteration for the nonlinear solution. A force norm convergence tolerance of 0.03 was used.

5.0 Creep analysis of a thick walled cylinder

A suddenly applied pressure is applied to the inside of a thick cylinder and the creep response is calculated. The plane strain cylinder has an inside radius of 4.064×10^{-3} m and a outside radius of 6.35×10^{-3} m. Six elements are used to model the cylinder through the thickness. An internal pressure is applied as a function of time as shown in Figure 18. Load steps of 6 seconds were taken. The material constants for equation (74) are $A_1 = 8.27 \times 10^{-3}$, $A_2 = 4.4$ and $A_3 = 0.0$ with a Young's modulus of 137 GPa and a Poisson's ratio of 0.3. Shown in Figure 19 are the resulting effective stress as a function of time at $r = 4.25 \times 10^{-3}$ m and $r = 6.16 \times 10^{-3}$ m. A force convergence tolerance of 0.001 was used. A viscosity coefficient of 20/3 was necessary to control the hourglass modes. The results compare favorably to a steady state solution reported in [34].

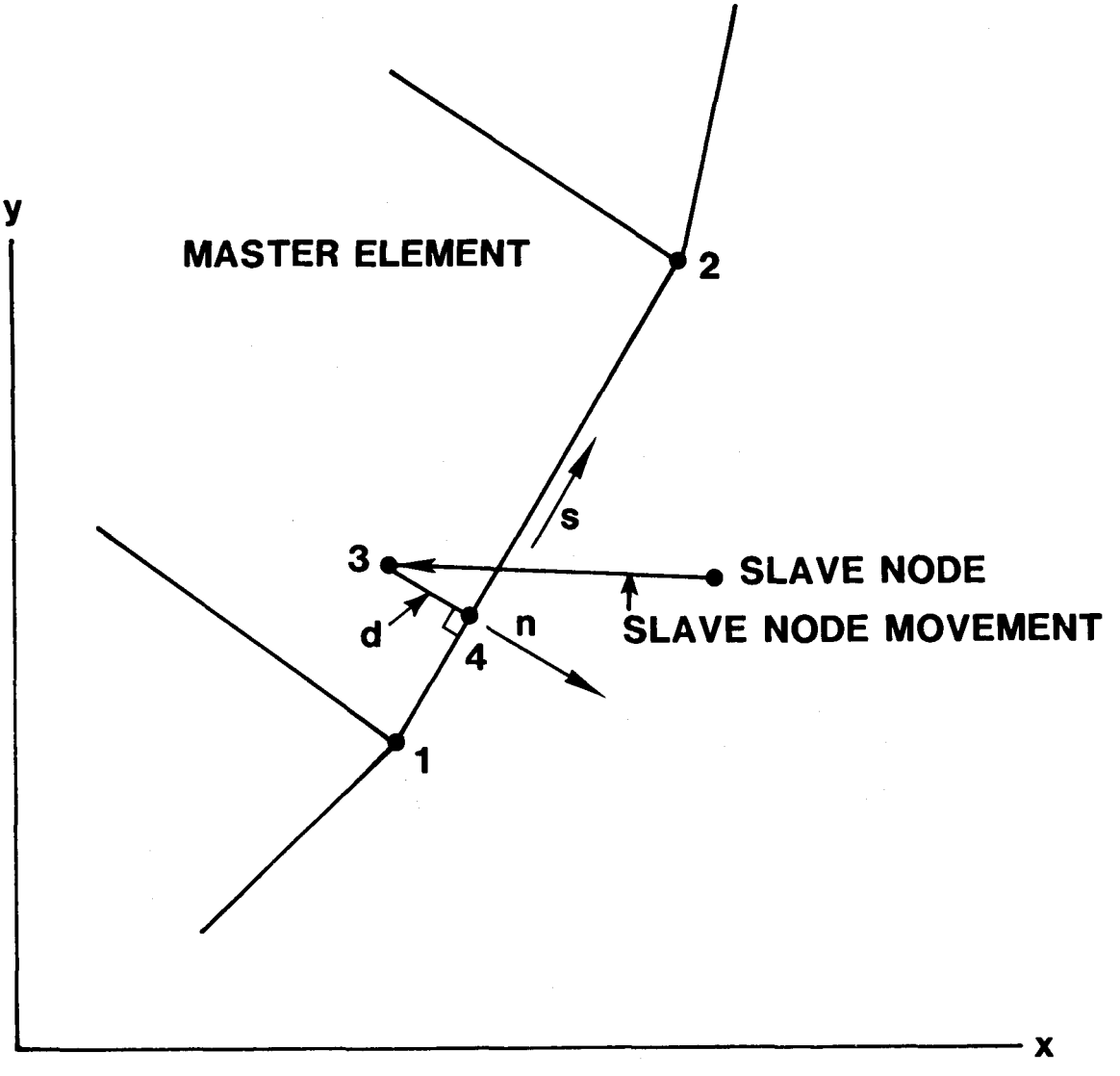

Figure 1. Master-Slave Relationships for Sliding Interfaces

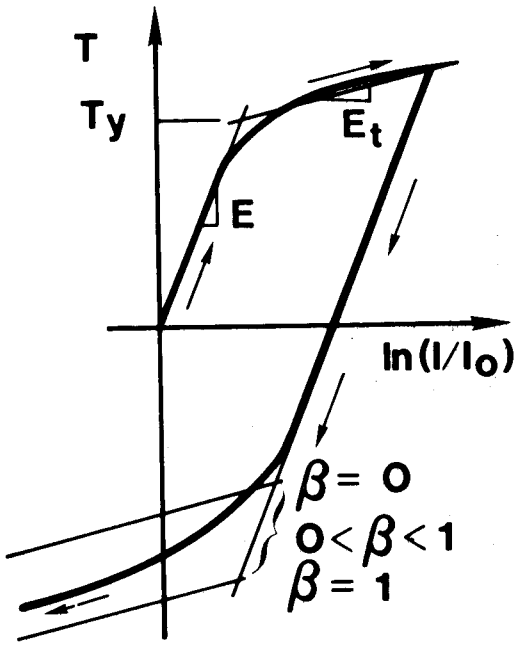

Figure 2. Typical behavior of a ductile metal bar loaded first in uniaxial tension followed by uniaxial compression. The straight line approximation is characterized with an elastic modulus E, a yield stress T_y, a strain hardening modulus E_t, and a hardening paramameter β. Kinematic hardening is obtained with β = 0, isotropic hardening is obtained with β = 1, and a linear combination of the two is obtained for β between zero and one.

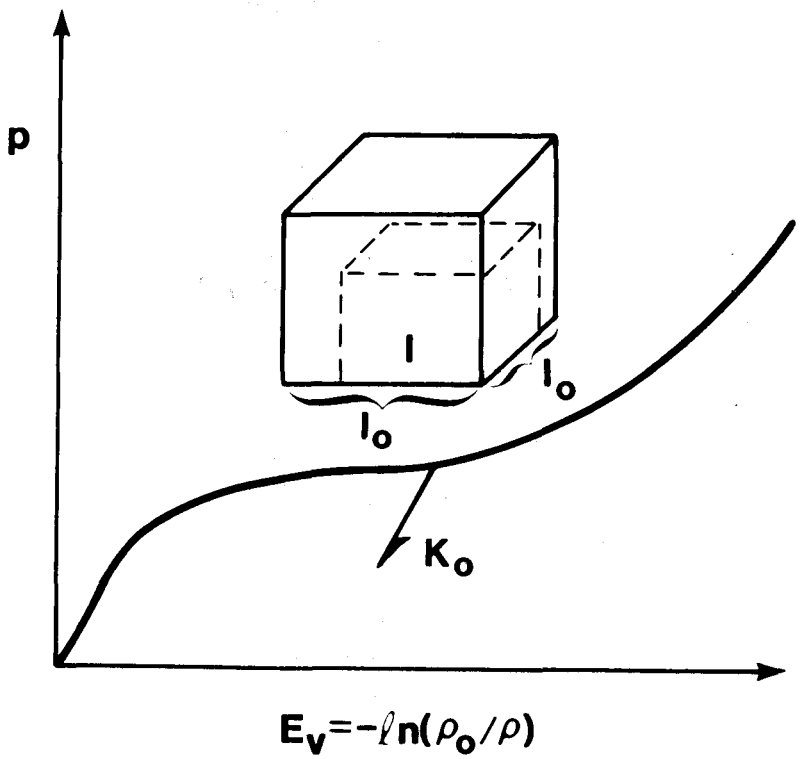

Figure 3. Pressure versus volume strain behavior for a porous material. Unloading is assumed to occur elastically with a modulus of K_0.

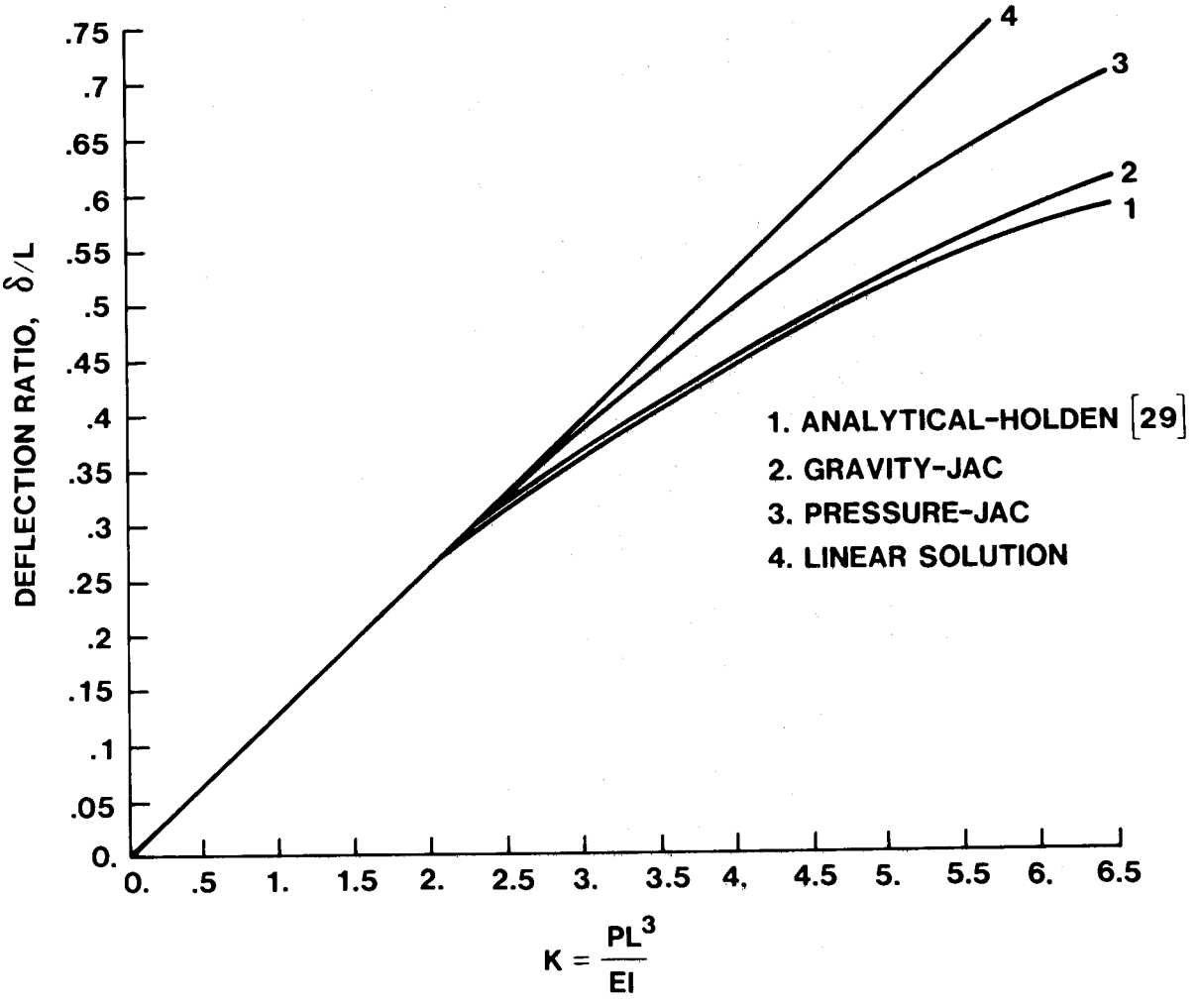

Figure 4. Load vs. deflection curve for the cantilever beam analysis.

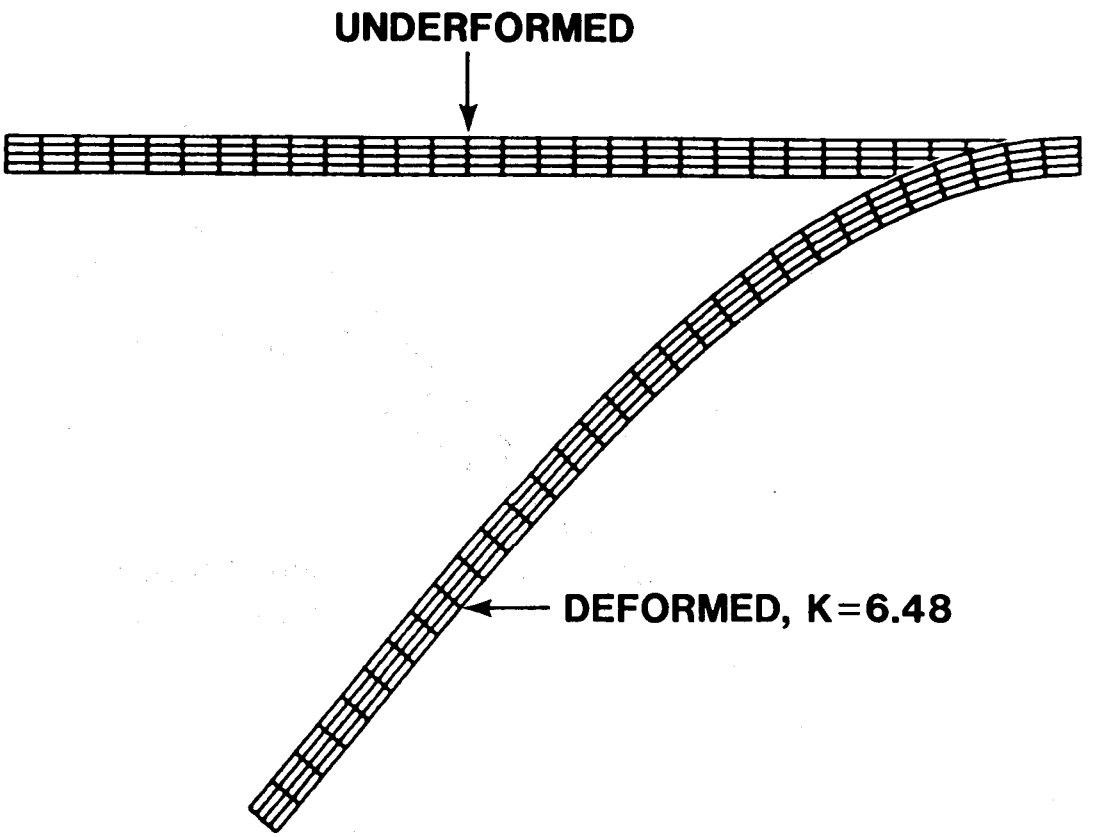

Figure 5. Undeformed and deformed mesh due to gravity load at K = 6.48 for cantilever beam problem.

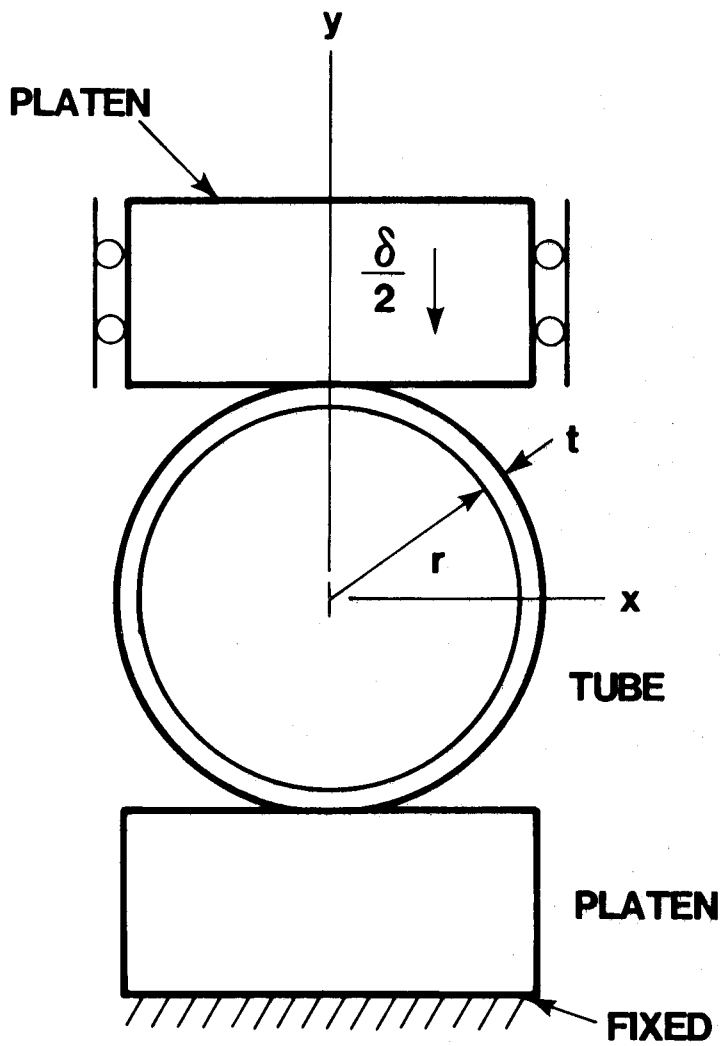

PROPERTIES OF TUBE

$r = 0.0238m$

$t = 0.00325m$

$E = 68.9\,GPa$

$E_t = 117.1\,MPa$

$T_y = 68.9\,MPa$

$\nu = 0.3$

$\beta = 0$

Figure 6. Geometry and material properties for the tube crushing problem.

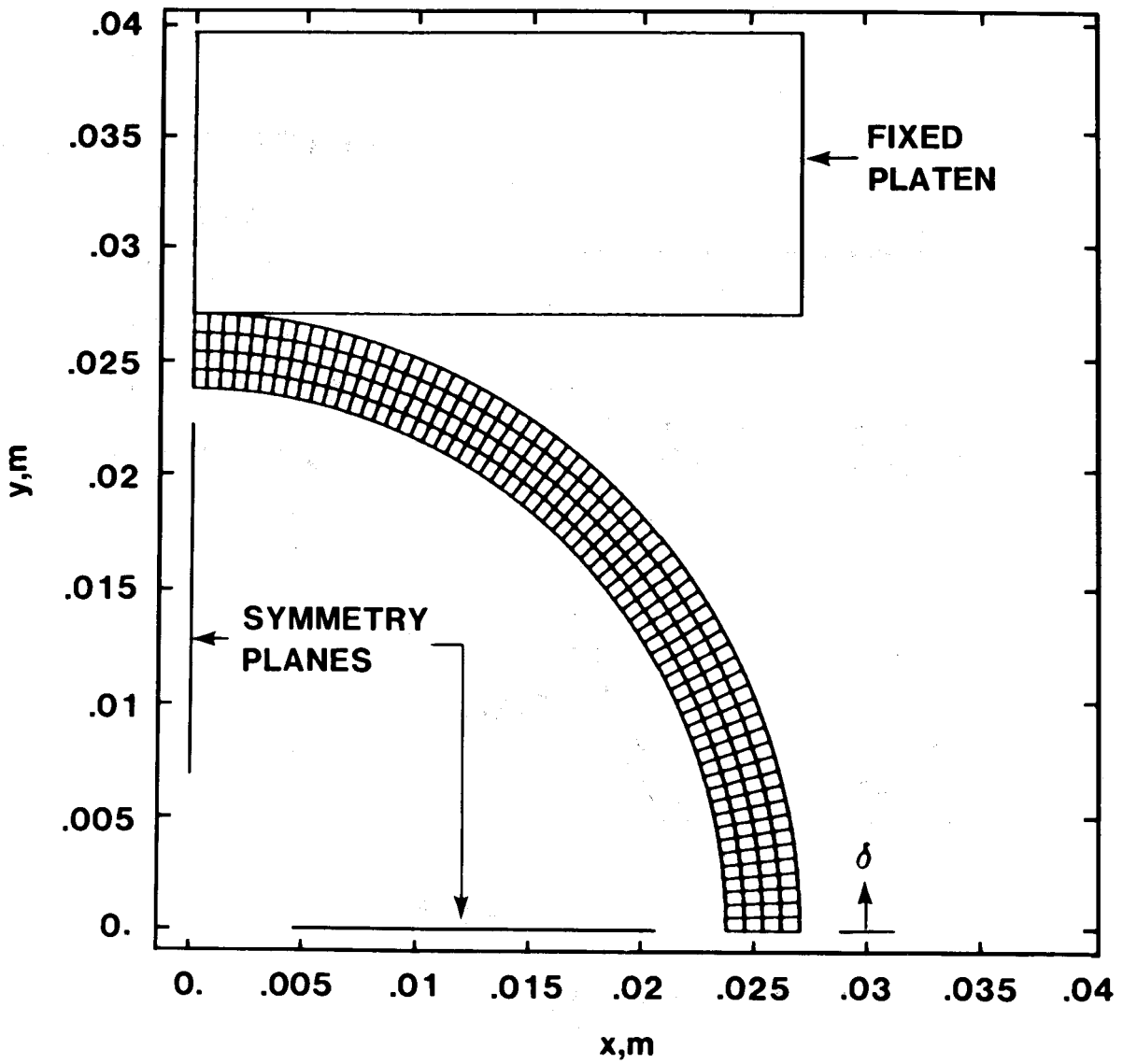

Figure 7. Finite element model for tube crushing problem.

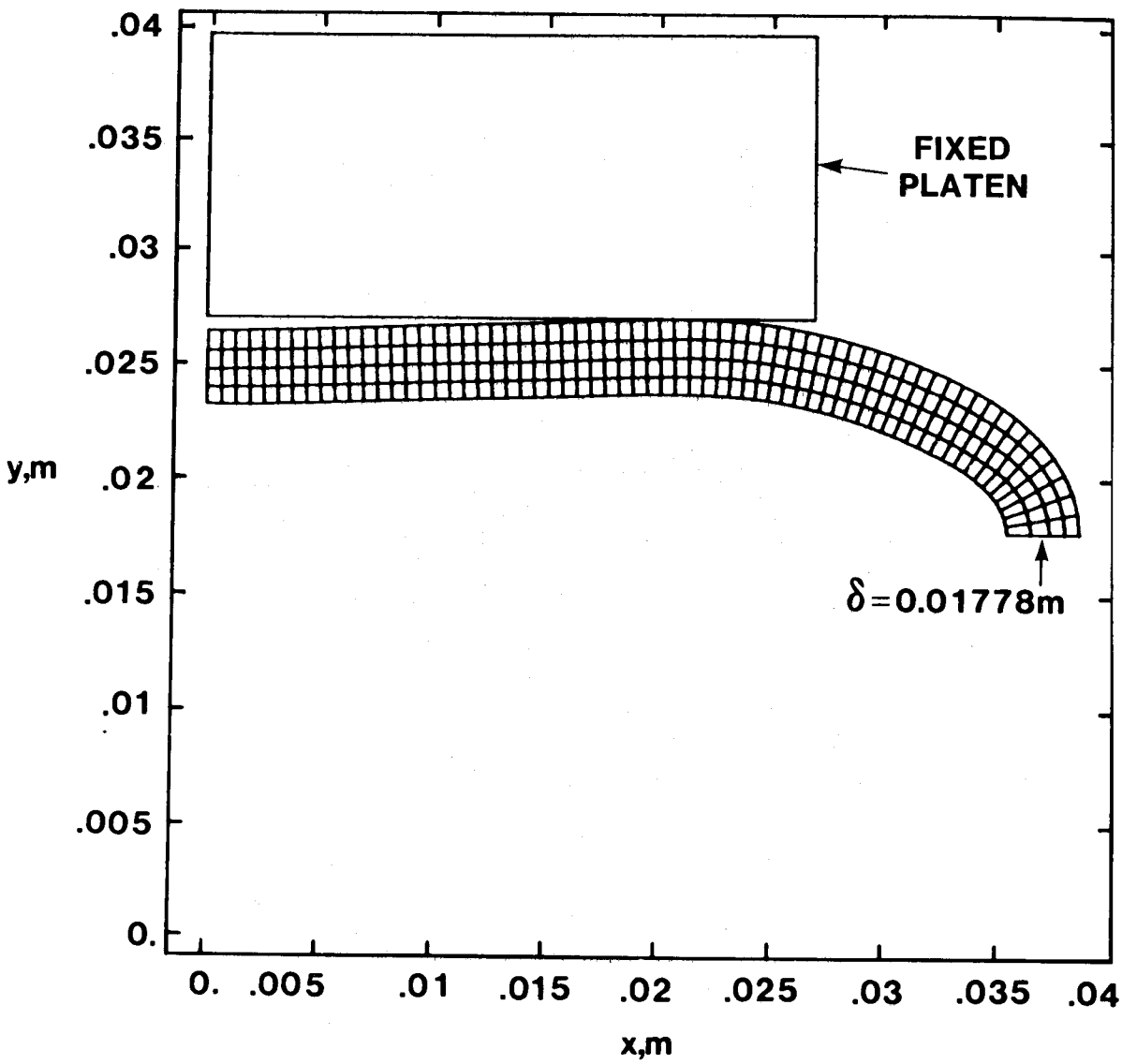

Figure 8. Deformed shape plot of the tube crushing problem at a displacement of δ = 0.01778 m.

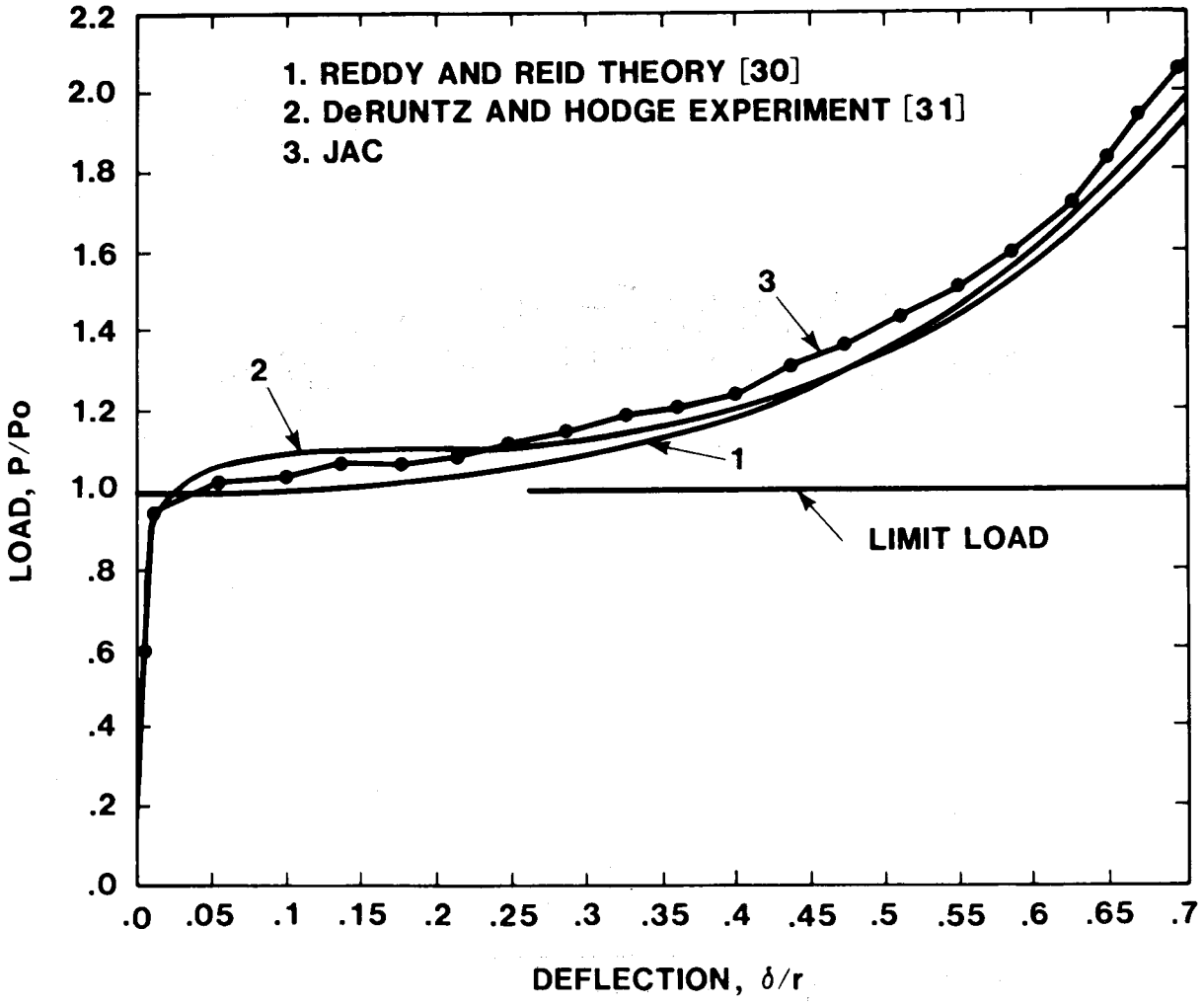

Figure 9. Load vs. deflection curves for tube crushing problem.

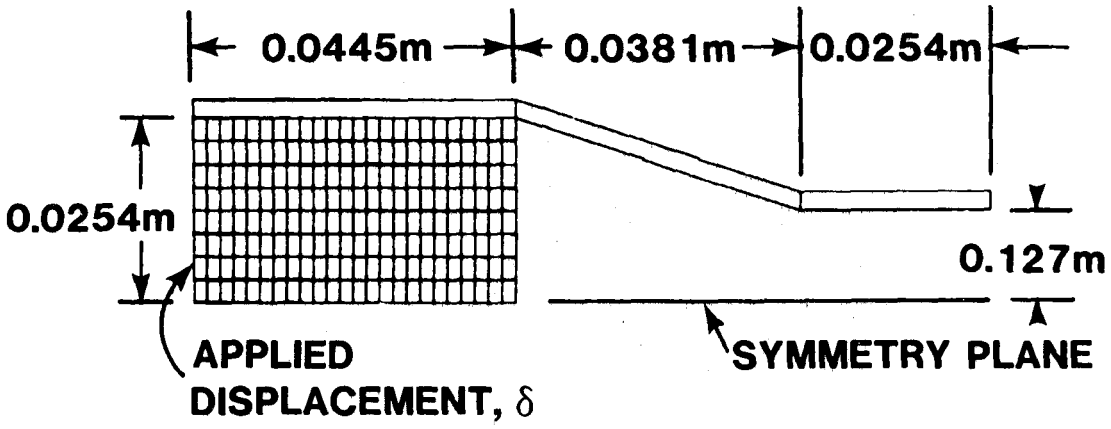

MATERIAL PROPERTIES

$E = 68.9$ GPa

$\nu = 0.3$

$T_y = 68.9$ MPa

$E_t = 0.0$ Pa

$\beta = 0$

Figure 10. Geometry, material properties and finite element mesh of extrusion problem.

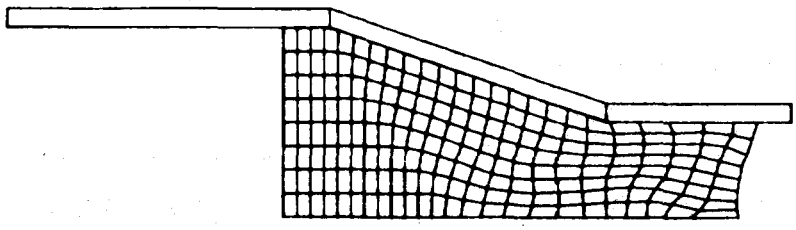

Figure 11. Deformed mesh of the plane strain analysis of the extrusion problem at an applied displacement of 0.381 m.

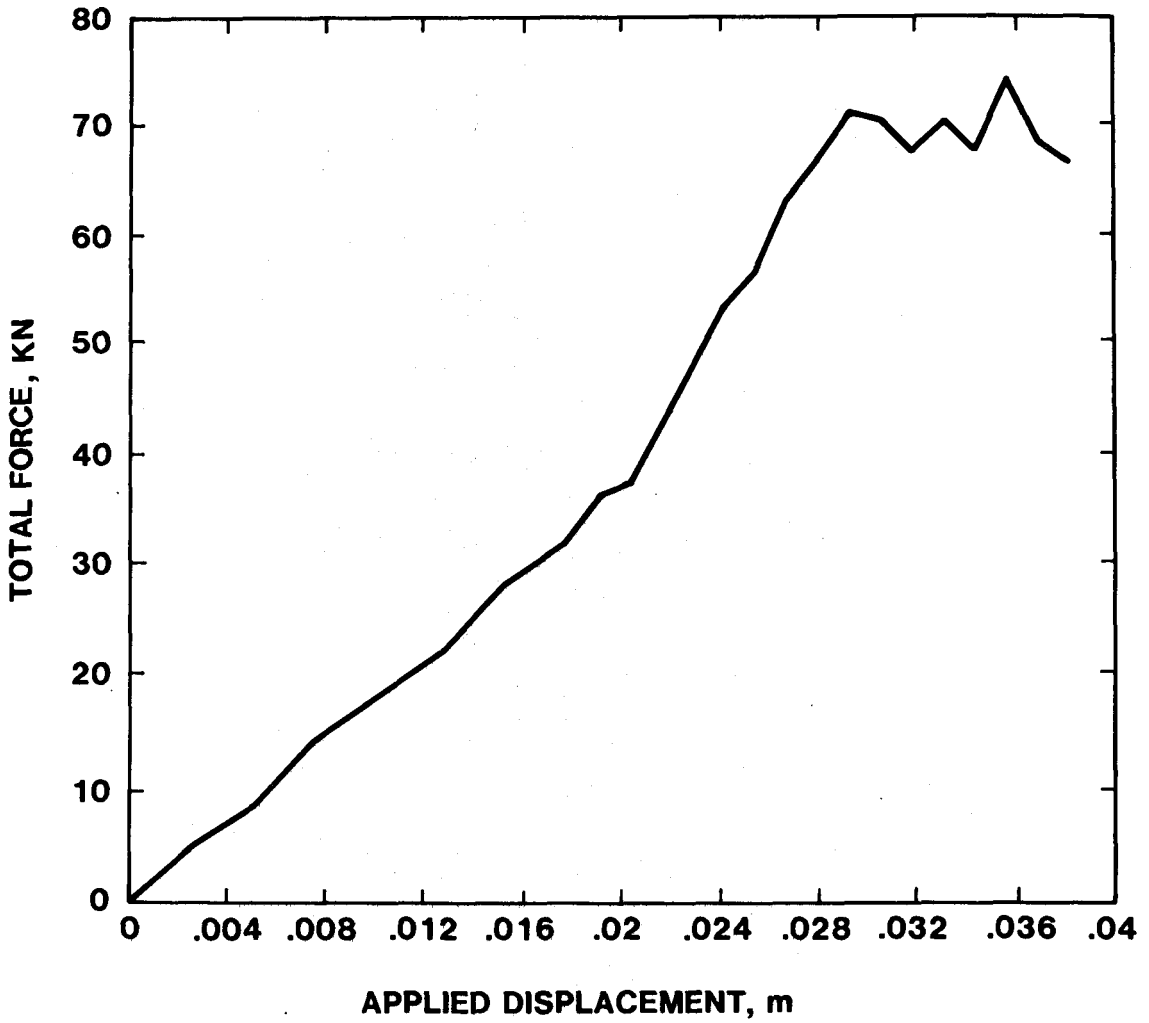

Figure 12. Total force vs. applied displacement curve for the plane strain analysis of the extrusion problem.

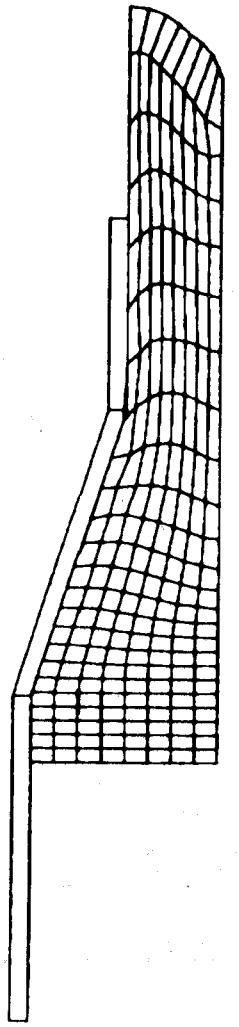

Figure 13. Deformed mesh of the axisymmetric analysis of the extrusion problem at an applied displacement of 0.356 m.

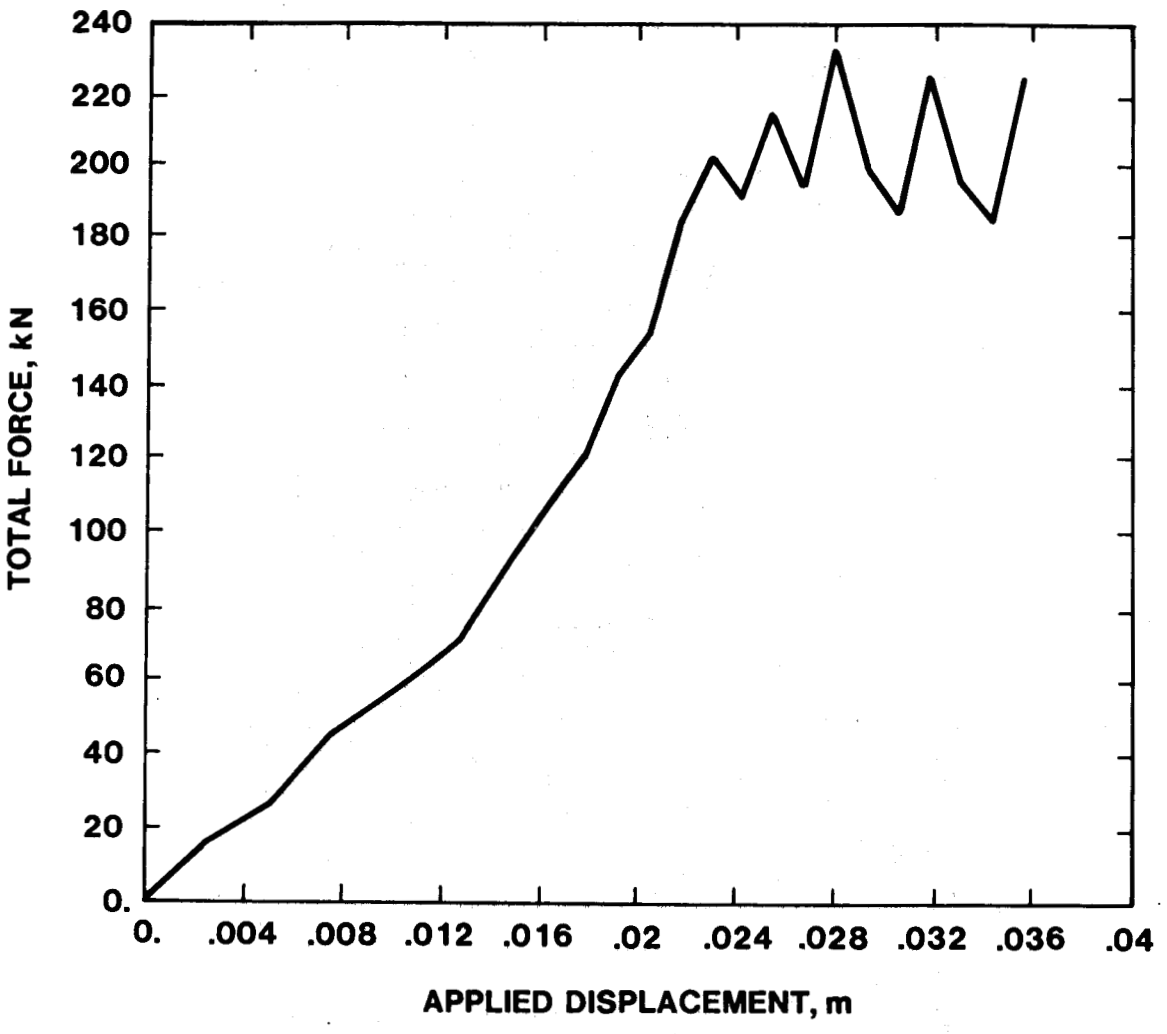

Figure 14. Total force vs. applied displacement curve for the axisymmetric analysis of the extrusion problem.

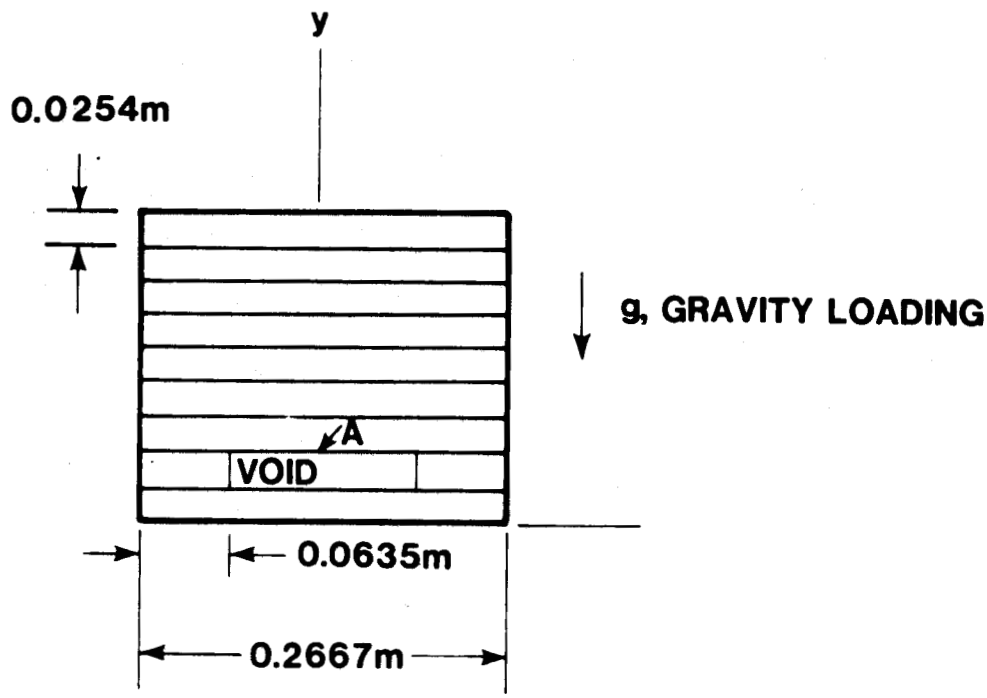

LOAD SEQUENCE

1. 1g
2. 26.0g
3. 50.2g
4. 75.2g
5. 150.2g

MATERIAL PROPERTIES

$E = 3.17\text{GPa}$

$\nu = 0.3$

$\rho = 14.305\ \text{kN/m}^3$

Figure 15. Description of sliding beam problem.

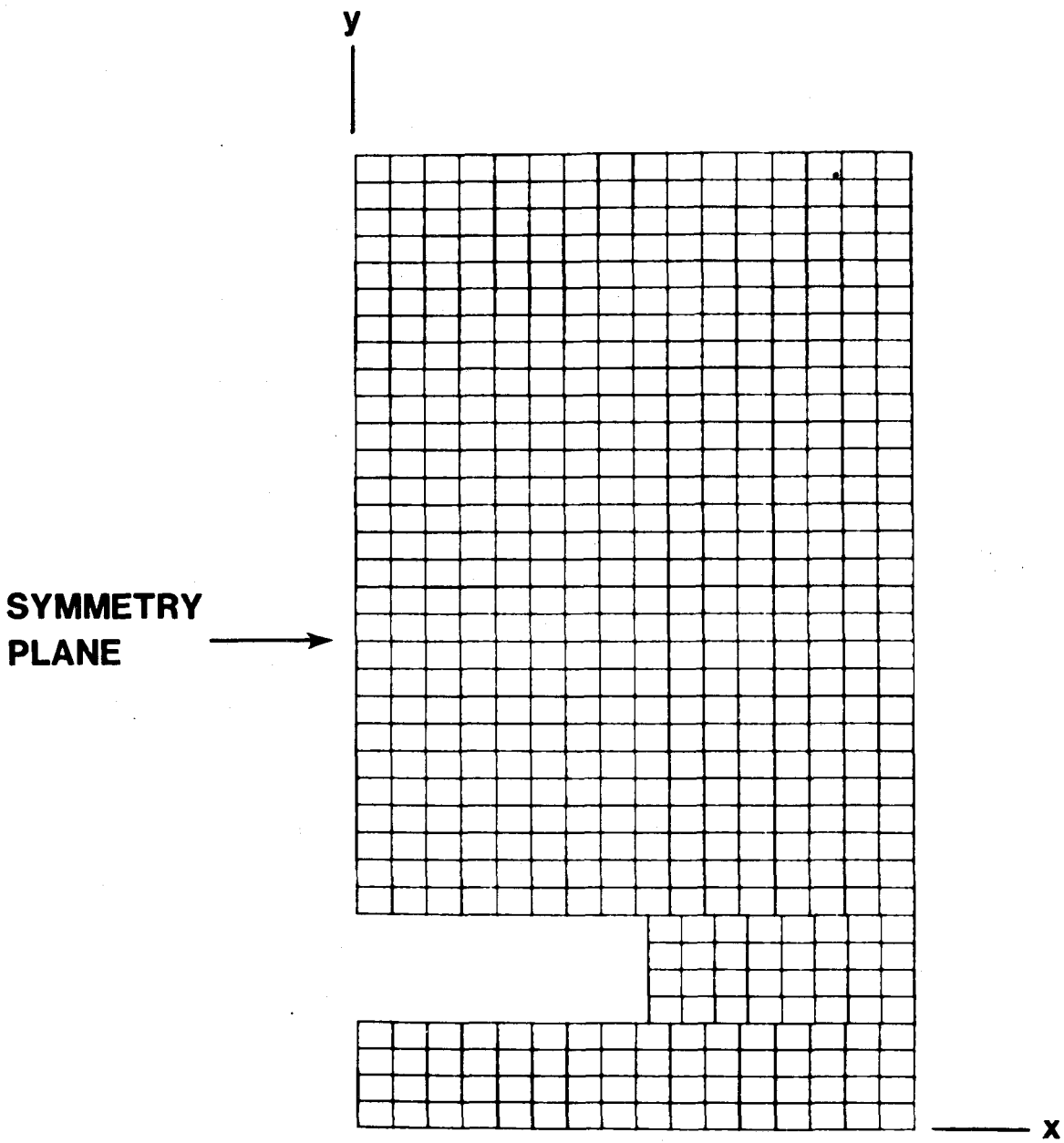

Figure 16. Finite element mesh of the sliding beam problem.

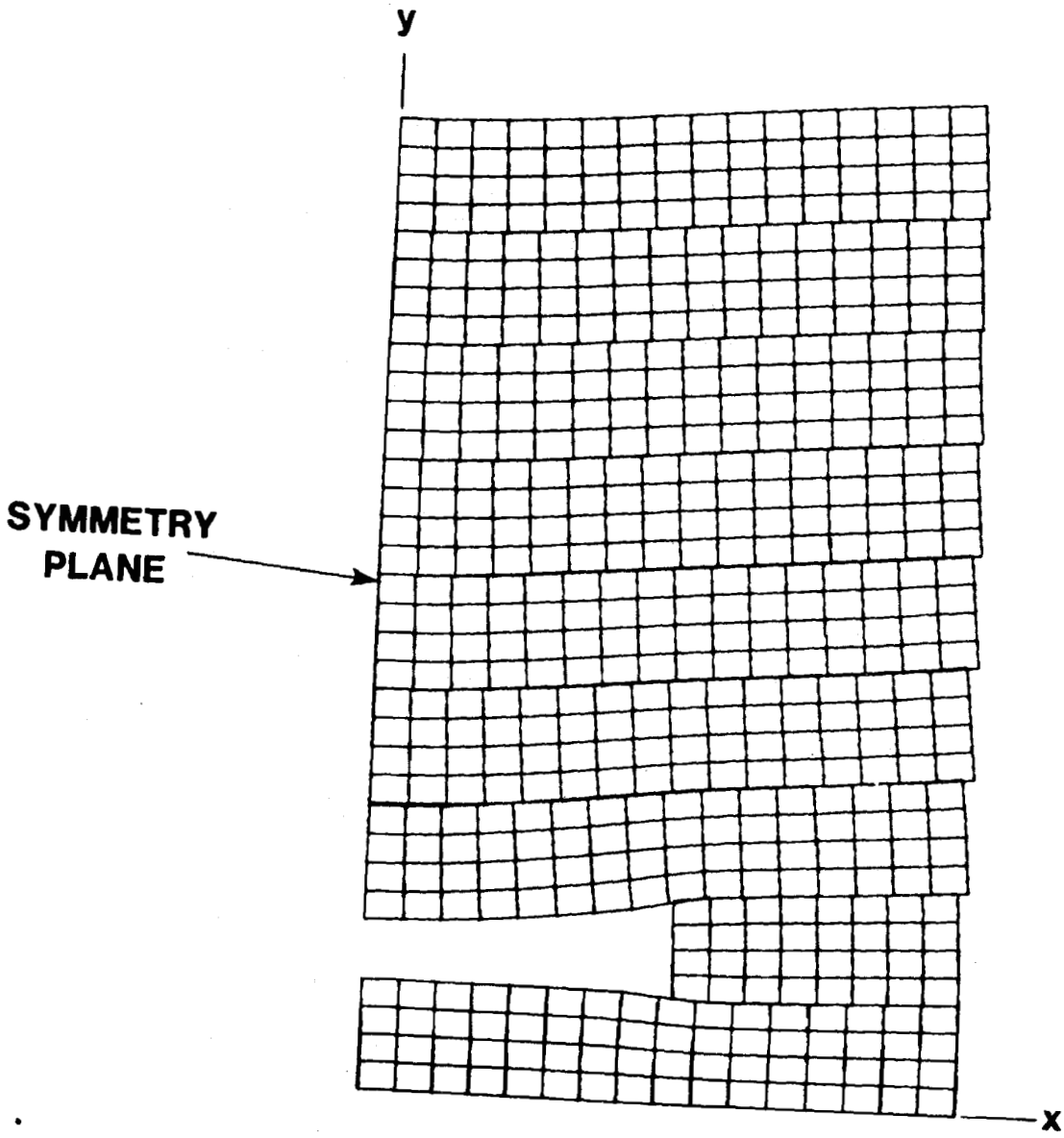

Figure 17. Deformed mesh plot of the sliding beam problem with the displacements magnified 200 times.

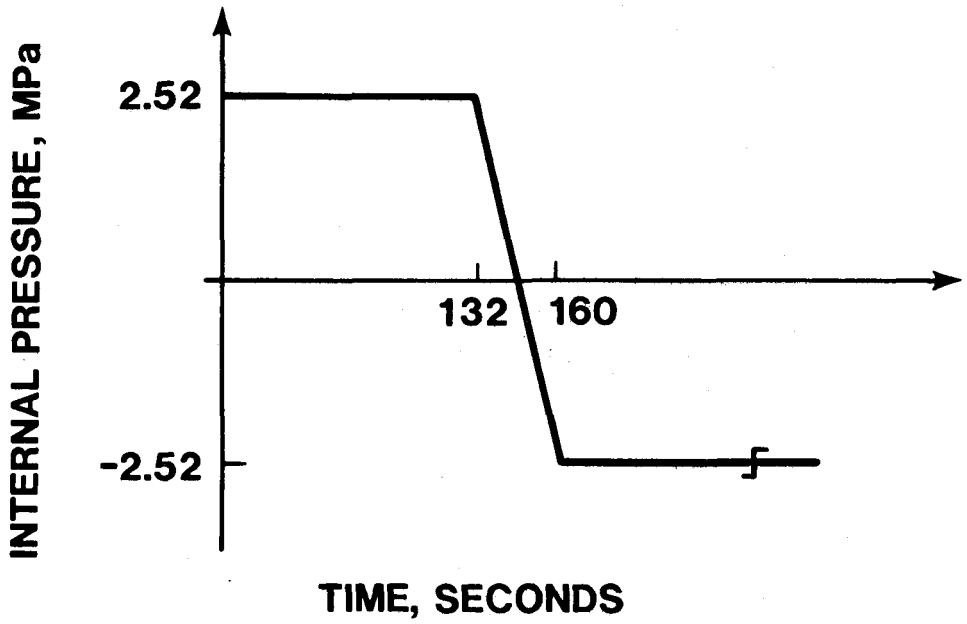

Figure 18. Input pressure vs. time curve for the cyclic creep analysis of a thick walled cylinder.

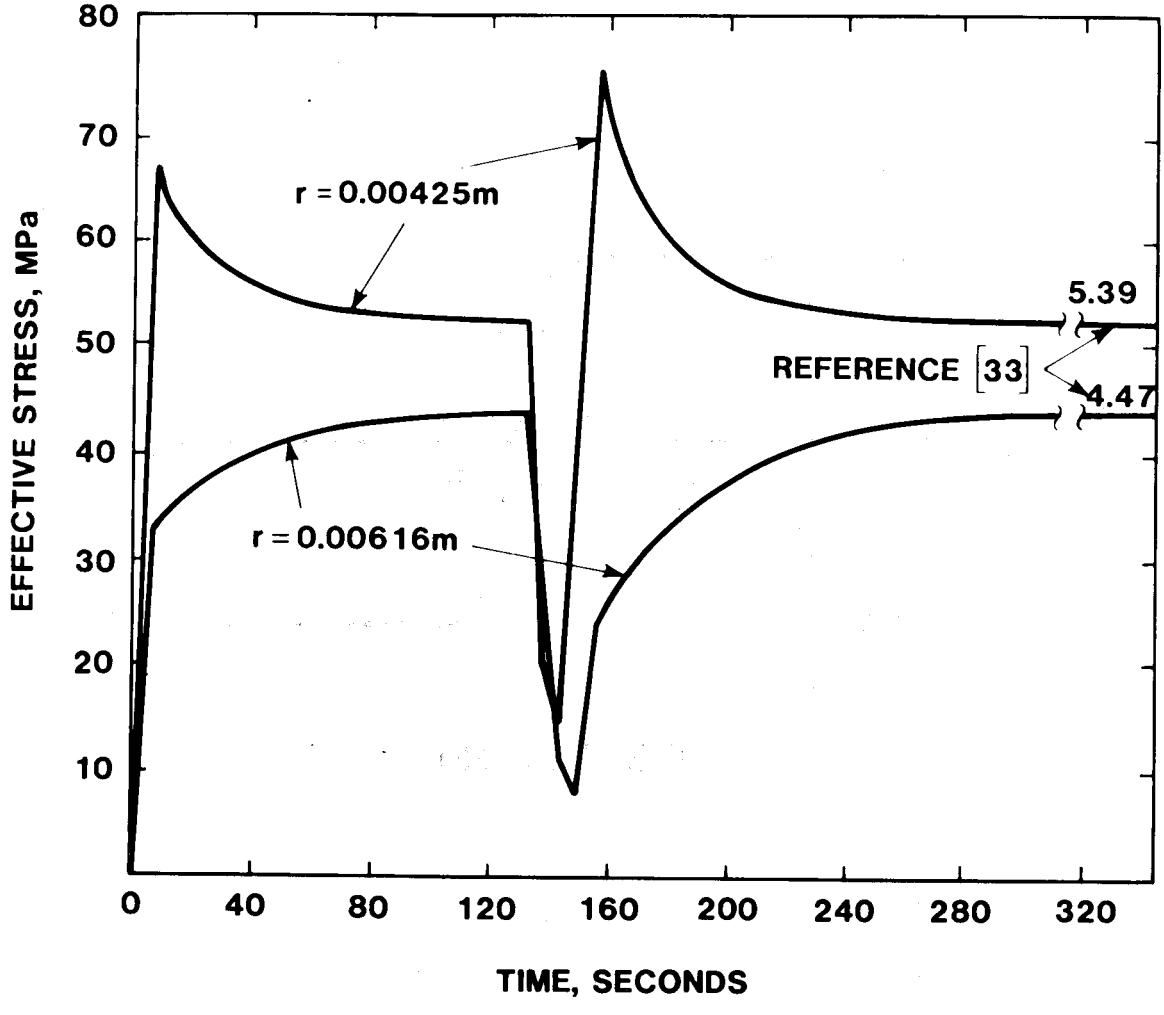

Figure 19. Effective stress vs. time curves for the cyclic creep analysis of a thick walled cylinder.

VII. REFERENCES

1. Bathe, K. J. "ADINA - A Finite Element Program for Automatic Dynamic Incremental Nonlinear Analysis, Acoustics and Vibration Laboratory, Mechanical Report 82448-1, Engineering Department, MA. Institute of Technology, Cambridge, MA, September 1975, (Revised 1977).

2. MARC-CDC, General Purpose Finite Element Analysis Program, Control Data Corporation, Minneapolis, MN. Publication No. 17309500, Rev. J.

3. Key, S. W., "A Finite Element Procedure for the Large Deformation Dynamic Response of Axisymmetric Solids," Computer Methods in Applied Mechanics and Engineering, April 1974, pp. 195-218.

4. Biffle, J. H. and Gubbels, M. H., "WULFF - A Set of Computer Programs for the Large Displacement Dynamic Response of Three Dimensional Solids," Sandia National Laboratories, Albuquerque, New Mexico, SAND76-0046, 1976.

5. Hallquist, J. O., "User's Manual for DYNA2D - - An Explicit Two-Dimensional Hydrodynamic Finite Element Code with Interactive Rezoning," Lawrence Livermore National Laboratory, Livermore, CA, Report UCID-18756, Rev. 1, February 1982.

6. Hallquist, J. O., "User's Manuals for DYNA3D and DYNAP," Lawrence Livermore National Laboratory, Livermore, CA, Report UCID-19156, July 1981.

7. Belytschko, T., and Robinson, R. R., "SAMSON2: A Nonlinear Two-Dimensional Structure/Media Interaction Computer Code," Report AFWL-TR-81-109, Kirtland AFB, New Mexico, November 1981.

8. Irons, B. and Elsawaf, A., "The Conjugate Newton Algorithm for Solving Finite Element Equations," Formulations and Computation Algorithms in Finite Element Analysis, Eds. K. J. Bathe, J. T. Oden, and W. Wunderlich, MIT Press 1977.

9. Hestenes, M. R., and Stiefel E., "Methods of Conjugate Gradients for Solving Linear Systems," Journal of Research of the National Bureau of Standards, Vol. 49., No. 6 December 1952, pp. 409-436.

10. Ralston, A. and Wilf, H. S., Mathematical Methods of Digital Computers, John Wiley & Sons, Inc., N.Y. 1960.

11. Consus, P., Golub, G. H., and O'Leary D. P., "A Generalized Conjugate Gradient Method for the Numerical Solution of Elliptic Partial Differential Equations," Sparse Matrix Computations, Ed. Bunch, J. R., and Rose, D. J., Academic Press N.Y. 1965, pp. 307-332.

12. Fletcher, R., and Reeves, C. M., "Functional Minimization by Conjugate Gradients," The Computer Journal 7 1964, pp. 149-154.

13. Lenard, M. L., "Convergence Conditions for Restarted Conjugate Gradient Methods with Inaccurate Line Searches," Mathematical Programming 10 1976, pp. 32-51.

14. Powell, M. J. D., "Restart Procedures for the Conjugate Gradient Method," Mathematical Programming 12 1977, pp. 242-254.

15. Daniel, J. W., "The Conjugate Gradient Method for Linear and Nonlinear Operator Equations," SIAM Journal of Numerical Analysis, Vol. 4 No. 1 1967, pp. 10-26.

16. Bartels, R. and Daniel, J. W., "A Conjugate Gradient Approach to Nonlinear Elliptic Boundary Value Problems in Irregular Regions," Lecture Notes in Mathematics, Ed. A. Dold and B. Eckmann, Springer-Verlay, New York 1973.

17. Malvern, L. E., Introduction to the Mechanics of a Continuous Medium, Prentice-Hall, Inc., Englewood Cliffs, New Jersey, 1969.

18. Biffle, J. H., and Key S. W., "Finite Element Formulations for Transient Dynamic Problems in Solids Using Explicit Time Integrations," Computer Methods in Applied Mechanics and Engineering 12 1977, pp. 323-336.

19. Hallquist, J. O., "NIKE2D: An Implicit, Finite-Deformation, Finite Element Code for Analyzing the Static and Dynamic Response of Two-Dimensional Solids," Lawrence Livermore National Laboratory, Livermore, CA, Report UCRL-52678, March 3, 1979.

20. Hughes, T. J. R., and Winget, J., "Finite Rotation Effects in Numerical Integration of Rate Constitutive Equations Arising in Large-Deformation Analysis," International Journal Numerical Methods in Engineering 1980, Vol. 15, pp. 1862-1867.

21. Johnson, G. C., and Bammann, D. J., "A Discussion of Stress Rates in Finite Deformation Problems," International Journal of Solids and Structures, in review.

22. Atluri, Satya M., "On Constitutive Relations at Finite Strain: Hypo-elasticity and Elasto-Plasticity with Isotropic and Kinematic Hardening," Georgia Institute of Technology, Atlanta, Georgia, Report No. GIT-CA CM-SNA-83-16, February 1983.

23. Defalias, Y. F., "Corotational Rates for Kinematic Hardening at Large Plastic Deformations," Univ of California at Davis, Report No. 82-1, April 1982.

24. Goudeau, G. L. and Hallquist, J. O., "Recent Developments in Large-Scale Finite Element Lagrangian Hydrocode Technology," Computer Methods in Applied Mechanics and Engineering 1982, Vol. 33, Nos. 1-3, pp. 725-757.

25. Flanagan, D. P. and T. Belytschko, "A Uniform Strain Hexahedron and Quadrilateral with Orthogonal Hourglass Control," International Journal for Numerical Methods in Engineering 1982, Vol. 17, pp. 679-706.

26. Flanagan, D. P., "The Uniform Strain Axisymmetric Quadrilateral," Internal Memorandum, Sandia National Laboratories, Albuquerque, New Mexico, April 1982.

27. R. D. Krieg and S. W. Key, "Implementation of a Time Independent Plasticity Theory Into Structural Computer Programs," in: J. A. Stricklin and K. J. Saczalski (eds)., Constitutive Equations in Viscoplasticity: Computational and Engineering Aspects, AMD Vol. 20, (The American Society of Mechanical Engineers, New York 1976), pp. 125-248.

28. R. D. Krieg, "An Efficient Numerical Method for Time Independent Plasticity," Sandia National Laboratories, Albuquerque, New Mexico, SAND77-0943, 1977.

29. R. D. Krieg and D. B. Krieg, "Accuracies of Numerical Solution Methods for the Elastic-Perfectly Plastic Model, Journal of Pressure Vessel and Piping, November 1977, Vol. 99, pp. 510-515.

30. Krieg, R. D., "A Simple Constitutive Description for Soils and Crushable Foams," Sandia National Laboratories, Albuquerque, New Mexico, Report No. SC-DR-72-0883, 1972.

31. Holden, J. T., "On the Finite Deformations of Thin Beams," International Journal of Solids and Structures 1982, Vol. 8, pp. 1051-1055.

32. Reddy, T. Y., and Reid, S. R., "On Obtaining Properties from the Ring Compression Test," Nuclear Engineering and Design 52 1977, pp. 257-263.

33. Key, S. W., Krieg, R. D., and Bathe, K. J., "On the Application of the Finite Element Method to Metal Forming Pressures - Part I," Computer Methods in Applied Mechanics and Engineering, November 18, 1979, pp. 597-608.

34. DeRuntz, J. A., Jr., and P. G. Hodge, Sr., "Crushing of a Tube Between Rigid Plates," Journal of Applied Mechanics, September 1963, pp. 391-365.

35. Sutherland, H. J., eta, "Physical Simulations of Subsidence by Centrifuge Techniques," 20th U. S. Symposium on Rock Mechanics, Austin, Texas, June 4-6, 1979.

36. Finnie, I. and W. R. Heller, Creep of Engineering Materials, McGraw-Hill 1959, pp. 208.

37. Jones, R. E., "User's Manual for QMESH, a Self-Organizing MESH Generator Program," Sandia National Laboratories, Albuquerque, New Mexico, Report SLA-74-0239, July 1974.

38. Beisinger, Z. E. and C. M. Stone, "TPLOT2: A Flexible X-Y Plotting Program for Use with Finite Element Software," Sandia National Laboratories, Albuquerque, New Mexico, SAND80-2508, February 1981.

39. Preece, D. S. and B. A. Lewis, "MOVIE-BYU User Document," Sandia National Laboratories, Albuquerque, New Mexico, SAND82-0945, September 1982.

40. Richgels, M. A. and J. H. Biffle, "ALGEBRA - A Computer Program that Algebraically Manipulates Finite Element Output Data," Sandia National Laboratories, Albuquerque, New Mexico, SAND80-2061, September 1980.

VIII. USER INSTRUCTIONS

The computer code JAC designed to be executed on the CRAY1 machine. It is normally used in conjunction with the four node two dimensional mesh generation programs QMESH [37], RENUM and QPLOT. The following input description requires a knowledge of the QMESH programs. Nodal and element flags which are used to define boundary conditions are output by the RENUM program on local file FT09 for input to the JAC program. The format of the FT09 file is noted in the QMESH document [37].

Output is written by JAC on the local file FT11 for use with the plot programs DETOUR, TPLOT2 [38], SPLOT, and MOVIE-BYU [39]. The program ALGEBRA [40] may be used to algebraically manipulate the output data. DETOUR plots contours and deformed mesh plots for two dimensional bodies. TPLOT2 is a function versus time plot program. SPLOT plots functions versus prescribed distances in either two or three dimensional bodies and MOVIE-BYU can be used to plot contours, deformed meshes and color fringe patterns of variables.

Functions versus time are input which define all the quantities used to control the solution. Changing boundary conditions, print and plot increments, and solution strategy are controlled by functions.

JAC Input File FT05 Description

1. Title Card (8A10)

Col's	Fmt	Var	Item
1-80	A	TITLE	Any title suitable for identifying the data deck and the program output.

2a. Control Card One (13I5,5X,E10.0)
(Table 2 contains a brief description of the two control cards.)

Col's	Fmt	Var	Item
1-5	I	NUMMAT	Total number of different materials. See Section 3.
6-10	I	NUMFT	Total of load and solution control functions which are input; NUMFT $\leq$ 10. See Section 4.
11-15	I	NUMPL	Maximum number of points to describe any one of the NUMFT functions. See Section 4.
16-20	I	NUMPC	Number of boundary condition cards.
21-25	I	NSS	Number of sliding interfaces.
26-30	I	NAXIS	Geometry parameter If NAXIS = 0, plane strain geometry. If NAXIS $\neq$ 0, axisymmetric geometry. Radial displacement at r = 0 must be set equal to zero with boundary condition cards. Concentrated forces are input as force per radian.
31-35	I	NOUT	Output print function number. If NOUT = 0, output will be printed every time step. If NOUT $\neq$ 0, a type 2 function is used, as described in Table 3, to calculate time intervals at which all the current coordinates displacements, and stresses will be printed.

36-40	I	NSOLT	Solution control function number. A type 2 function is used, (Table 3) to calculate solution time increments. The starting time for the solution is the first time in the NSOLT function and the final time of the problem is the last time in the NSOLT function.
41-45	I	NODE4	Iterative solution control. If NODE4 = 1, a geometrically linear and material nonlinear solution will be obtained for each load step. If NODE4 = 2, a geometric and material nonlinear solution will be obtained for each load step. If NODE4 = 3, during each load step a solution is first obtained with linear geometry and nonlinear material properties. Then a second solution is obtained with both non-linear geometry and material properties by using the first solution to start the second solution. Default = 2.
46-50	I	NODE4F	NODE4 value function number. If NODE4F = 0, the value on NODE4 in columns 41-45 is used to control the iterative procedure. If NODE4F $\neq$ 0, function NODE4F is used to determine the value of NODE4 during the solution process. Values of 1,2 or 3 are permissible for the value of the NODE4F function. A type 3 function is used (Table 3).

51–55	I	NDISP	Initial starting incremental displacement vector control. If NDISP = 0, at the beginning of each load step, the assumed incremental displacement vector to start the iteration procedure is zero. If NDISP ≠ 0, at the beginning of each load step, function NDISP is used to obtain a ratio, represented by the value of the function at the beginning of the load step. An incremental displacement vector is then calculated by multiplying the incremental displacement vector of the previous load step by the ratio. A type 3 function is used (Table 3).
56–60	I	NIMAX	Maximum number of iterations allowed per load step for each iterative solution specified by the NODE4 parameter. Default = number of degrees of freedom.
61–65	I	NTERM	Temperature problem control. If NTERM = 0, isothermal problem is solved. If NTERM = 1, temperature dependent problem is solved with temperatures input on FT58. The format for FT58 is WRITE(58)TIME, (T(I),I=1,NUMNP) where T is the nodal temperature and NUMNP is the total number of nodal points.
71–80	E	VISCO	Hourglass viscosity parameter. If VISCO = 0, default = 1.0. To approximate a zero viscosity parameter a small value must be input.

2b. Control Card Two (5I5)

Col's	Fmt	Var	Item
1- 5	I	NGRAVX	x or r direction body force function number. If NGRAVX = 0, no body force loads or centrifugal forces are applied in the x or r direction. If NGRAVX ≠ 0, function number NGRAVX is used to define the magnitude of the x body force load or the r centrifugal forces. For x body force loads, Load = Density*volume*f(t). For centrifugal forces, Load = Density*volume*f(t)*r where f(t) represents the square of the angular velocity. Volume and r is supplied by the program and density is input on material cards. A type 1 function is used (Table 3).
6-10	I	NGRAVY	y or z direction body force function number. If NGRAVY = 0, no body force loads in the y or z direction are applied. If NGRAVY ≠ 0, function number NGRAVY is used to define the magnitude of the y or z body force load. Load = Density*volume*f(t). Volume is supplied by the program and density is input on material cards. A type 1 function is used (Table 3).

11-15	I	NSTRTR	Restart read parameter. If NSTRTR = 0, problem is not a restart problem. If NSTRTR = 1, problem is a restart problem and the start time TSTART, is the first time of solution function NSOLT. The problem will be started at the time which is found to FT32 that is greater than or equal to TSTART. A problem is restarted by supplying a previously saved FT30 as FT32, see parameter NSTRTR on this card. The initial temperature under any starting conditions is obtained from FT58 if a thermal stress problem is to be calculated, NTERM = 1.
16-20	I	NPOUT	Plot output function number. If NPOUT = 0, data which can be plotted is written to FT11 at the end of each solution step. If NPOUT ≠ 0, a type 2 function is used (Table 3) to calculate time intervals at which FT11 is written.
21-25	I	NSTRTW	Restart function number. If NSTRTW = 0, data necessary to restart the problem is written to FT30 at the end of each solution step. If NSTRTW ≠ 0, a type 2 function is used (Table 2) to calculate time intervals at which FT30 is written.

TABLE 2.

Brief Control Card Description

2a. Control Card One (13I5,5X,E10.0)

Col's	Fmt	Var	Item	Default
1-5	I	NUMMAT	Number of different materials	0
6-10	I	NUMFT	Total number of functions	0
11-15	I	NUMPL	Maximum number of function points	0
16-20	I	NUMPC	Number of boundary condition cards	0
21-25	I	NSS	Number on sliding interfaces	0
26-30	I	NAXIS	Geometry parameter	0
31-35	I	NOUT	Output print function	0
36-40	I	NSOLT	Solution control function	0
41-45	I	NODE4	Iterative solution control	2
46-50	I	NODE4F	Iterative solution control function	0
51-55	I	NDISP	Starting vector function	0
56-60	I	NIMAX	Maximum number of iterations	NDOF
61-65	I	NTERM	Temperature control parameter	0
71-80	E	VISCO	Hourglass viscosity parameter	1.0

2b. Control Card Two (5I5)

Col's	Fmt	Var	Item	Default
1-5	I	NGRAVX	x or r direction body force function	0
6-10	I	NGRAVY	y or z direction body force function	0
11-15	I	NSTRTR	Restart read parameter	0
16-20	I	NPOUT	Plot output function	0
21-25	I	NSTRTW	Restart write function	0

Table 3.

JAC Function Description

Name	Variable	Type
Displacement	NF	1
Pressure	NF	1
X or R body force	NGRAVX	1
Y or Z body force	NGRAVY	1
Solution Control	NSOLT	2
Print Output Control	NOUT	2
Plot Output Control	NPOUT	2
Restart Write Control	NSTRTW	2
Iterative Solution Control	NODE4F	3
Starting Vector Control	NDISP	3

Note:

Type 1 Function - Interpolated Value Calculated

For a type 1 function, linear interpolation is used to find the value of the function at the current solution time which is between two time points of the function.

Type 2 Function - Time Increment Calculated

For a type 2 function, the value of the function at the beginning of a time increment represents the number of time subdivisions which will be used for the time increment.

Type 3 Function - Integer Value Calculated

For a type 3 function, the value of the function at the beginning of the time increment represents an integer number which will be held constant during the time increment.

3. Material Card Sets (NUMMAT sets)

Material Type 1 - Isothermal Elastic-Plastic

3a. Material Identification Card (2I5,3E10.0)

Col's	Fmt	Var	Item
1-5	I	N	Material property number
6-10	I	MTYPE(N)	Material type number
11-20	E	RO(N)	Density of material to be used for body force loads, force/length^3
21-30	E	BTIME(1,N)	Birth time at which elements with material number N become active. Default = 0.0.
31-40	E	BTIME(2,N)	Death time at which elements with material number N become inactive. Default = 1.0E100.

3b. Material Heading Card (8A10)

Col's	Fmt	Var	Item
1-80	A	——	User selected name of the material

3c. Material Stress Strain Information, 7 cards with (E10.0 format

Card	Col's	Fmt	Var	Item
1	1-80	E	(EE(I,1,N),I = 1,8)	Temperatures, θ
2	1-10	E	EE(1,2,N)	Young's modulus, E
3	1-10	E	EE(1,3,N)	Poisson's ratio, ν
4	1-10	E	EE(1,4,N)	Yield stress, T_y *
5	1-10	E	EE(1,5,N)	Hardening modulus, E_t
6	1-10	E	EE(1,6,N)	Hardening parameter, β
7	1-10	E	(EE(I,7,N),I = 1,8)	Thermal strains, D_θ

$0 \leq \beta \leq 1$

$\beta = 0$ kinematic

$\beta = 1$ isotropic

* If the yield stress $T_y = 0$, elastic behavior is assumed.

Material Type 2 - Temperature Dependent Elastic-Plastic

3a. Material Identification Card (2I5,3E10.0)

Col's	Fmt	Var	Item
1-5	I	N	Material property number
6-10	I	MTYPE(N)	Material type number
11-20	E	RO(N)	Density of material to be used for body force loads, force/length^3.
21-30	E	BTIME(1,N)	Birth time at which elements with material number N become active. Default = 0.0.
31-40	E	BTIME(2,N)	Death time at which elements with material number N become inactive. Default = 1.0E100.

3b. Material Heading Card (8A10)

Col's	Fmt	Var	Item
1-80	A	—	User selected name of the material

3c. Material Stress Strain Information 7 Cards of 8 values per card (8E10.0)

Card	Col's	Fmt	Var	Item
1	1-80	E	(EE(I,1,N),I=1,8)	Temperatures, θ
2	1-80	E	(EE(I,2,N),I=1,8)	Young's Moduli, E
3	1-80	E	(EE(I,3,N),I=1,8)	Poisson's ratio, ν
4	1-80	E	(EE(I,4,N),I=1,8)	Yield stresses, T_y
5	1-80	E	(EE(I,5,N),I=1,8)	Hardening Moduli, E_t
6	1-80	E	EE(1,6,N)	Hardening Parameter, β
7	1-80	E	(EE(I,7,N),I=1,8)	Thermal Strains, D_θ

$0 \leq \beta \leq 1$

$\beta = 0$ kinematic

$\beta = 1$ isotropic

* If the yield stress $T_y = 0$, elastic behavior is assumed.

Material Type 3 - Temperature Dependent Secondary Creep

3a. Material Identification Card (2I5,3E10.0)

Col's	Fmt	Var	Item
1-5	I	N	Material property number
6-10	I	MTYPE(N)	Material type number
11-20	E	RO(N)	Density of material to be used for body force loads, force/length^3
21-30	E	BTIME(1,N)	Birth time at which elements with material number N become active. Default = 0.0.
31-40	E	BTIME(2,N)	Death time at which elements with material number N become inactive. Default = 1.0E100.

3b. Material Heading Card (8A10)

Col's	Fmt	Var	Item
1-80	A	—	User selected name of the material

3c. Material Stress Strain Information, 7 cards with (8E10.0) Format

Card	Col's	Fmt	Var	Item
1	1-80	E	(EE(I,1,N),I=1,8)	Temperatures, θ
2	1-80	E	(EE(I,2,N),I=1,8)	Young's Moduli, E
3	1-80	E	(EE(I,3,N),I=1,8)	Poisson's Ratios, ν
4	1-10	E	EE(1,4,N)	Creep Law Constant, A_1
5	1-10	E	EE(1,5,N)	Creep Law Constant, A_2
6	1-10	E	EE(1,6,N)	Creep Law Constant, A_3
7	1-80	E	(EE(I,7,N),I=1,8)	Thermal Strains, D_θ

Material Type 3 - Temperature Dependent Secondary Creep (continued)

The creep law relating the effective strain rate, D_c, to the effective stress, σ_c, is

$$D_c = A_1 \sigma_c^{A_2} e^{-A_3/\theta}$$

The constants A_1 thru A_3 are constant with respect to temperature. E, ν, and D_θ are dependent upon temperature. If NTERM = 0, i.e., no temperatures are input, then $e^{-A_3/\theta}$ is equal to 1 and the values stored in EE(1,J,N,) are used.

Material Type 4 - Isothermal Finite Strain Soil and Crushable Foam

3a. Material Identification Card (2I5,3E10.0)

Col's	Fmt	Var	Item
1-5	I	N	Material property number
6-10	I	MTYPE(N)	Material type number
11-20	E	RO(N)	Density of material to be used for body force loads, force/length^3
21-30	E	BTIME(1,N)	Birth time at which elements with material number N become active. Default = 0.0.
31-40	E	BTIME(2,N)	Death time at which elements with material number N become inactive. Default = 1.0E100.

3b. Material Heading Card (8A10)

Col's	Fmt	Var	Item
1-80	A	---	User selected name of the material

3c. Material Stress Strain Information, (8E10.0) Seven Cards

Card	Col's	Fmt	Var	Item
1	1-80	E	(EE(I,1,N),I=1,8)	Temperatures, θ
2	1-10	E	EE(1,2,N)	Shear Modulus, G
2	11-20	E	EE(2,2,N)	Bulk Unloading Modulus, K
2	21-30	E	EE(3,2,N)	Yield Function Constant, A_1
2	31-40	E	EE(4,2,N)	Yield Function Constant, A_2
2	41-50	E	EE(5,2,N)	Yield Function Constant, A_3
3	1-10	E	EE(1,3,N)	Volumetric Strain, $\ln(\rho_o/\rho)$
3	11-20	E	EE(2,3,N)	Pressure, P
3	21-30	E	EE(3,3,N)	Volumetric Strain, $\ln(\rho_o/\rho)$
3	31-40	E	EE(4,3,N)	Pressure, P

Card	Col's	Fmt	Var	Item
4	1–10	E	EE(1,4,N)	Volumetric Strain, $\ln(\rho_o/\rho)$
4	10–20	E	EE(2,4,N)	Pressure, P
4	21–30	E	EE(3,4,N)	Volumetric Strain, $\ln(\rho_o/\rho)$
4	31–40	E	EE(4,4,N)	Pressure, P
.				
.				
.				
7	1–80	E	(EE(I,7,N),I=1,8)	Thermal Strains, D_θ

4. Function Cards. NUMFT Sets of Cards

4a. Function Control Card (2I5,A40)

Col's	Fmt	Var	Item
1-5	I	NF	Number of function
6-10	I	NFP	Number of function point pairs.
11-40	A	FTITLE	Description of functions, NODE4, OUTPUT, SOLUTION, for example.

4b. Function Value Cards (as many as needed) (8E10.0)

Col's	Fmt	Var	Item
1-10	E	P(1,NF,1)	Time
10-20	E	P(2,NF,1)	Value
.	.	.	.
.	.	.	.
.	.	.	.
.	E	P(1,NF,NFP)	Time
.	E	(P2,NF,NFP)	Value

5. Boundary condition cards (2I5,3E10.0)

Col's	Fmt	Var	Item
1-5	I	IFLAG	Number corresponding to flag number from QMESH.
6-10	I	NF	Number of function to be used. Type 1 interpolation will be used (Table 3).
11-20	E	CODE	Boundary condition code. If CODE = 0.0, x or r force specified, and y or z force specified. If CODE = 1.0, x or r displacement specified. If CODE = 2.0, y or z displacement specified. If CODE = 3.0, x or r, and y or z displacement specified. If CODE < 0.0, pressure specified. If CODE ≠ 1.0, 2.0, or 3.0, the value of CODE is the angle in degrees between the positive x or r direction and the direction of motion alone a sliding boundary. The normal displacement is zero and the tangential force is zero.
21-30	E	UX	Displacement, force or normal pressure in the x or r direction depending upon the value on CODE.
31-40	E	UY	Displacement, force or tangential pressure in the y or z direction depending upon the value on CODE.

NOTE: If axisymmetric geometry is used, concentrated forced are input as total force per radian. Also, at r = 0, the radial displacement must be set equal to zero.

6. Sliding Interface Condition Cards. NSS Cards (one for each sliding interface) (2I5,3E10.0,8I5)

Col's	Fmt	Var	Item
1- 5	I	IFLAGM(1)	QMESH flag number corresponding to first master side segment of sliding interface. Up to 8 additional master flags may be specified starting in column 41. Therefore, each slave segment can have a master segment which is specified by up to nine QMESH flags.
6-10	I	IFLAGS	QMESH flag number corresponding to slave side of sliding interface.
11-20	E	CF(1)	Coefficient of friction. If CF(1) < 0.0, surfaces are assumed to be fixed together upon contact.
21-30	E	CF(2)	Normal displacement tolerance. Surfaces are assumed to be in contact when the distances between surfaces is less than CF(2). Default = 1.0E-7.
31-40	E	CF(3)	Normal force tolerance. If the displacement tolerance is satisfied and if the normal force on the surface is less than CF(3), the surfaces are assumed to be in contact. Default = 1.0E100.
41-45	I	IFLAGM(2)	Additional master flags.
46-50	I	IFLAGM(3)	
.	.	.	
.	.	.	
76-80	I	IFLAGM(9)	

7. Convergence Control Card (I10,3E10.0)

Col's	Fmt	Var	Item
1-10	E	TOLU	Displacement norm convergence tolerance. Convergence is assumed, if $\left(\frac{\|\|\Delta u_{j+1}\|\| - \|\|\Delta u_j\|\|}{\|\|\Delta u_{j+1}\|\|}\right)^{1/2} \leq$ TOLU. where U is the incremental displacement during the load step, j is the iteration number and $\|\|A\|\|$ represents the L^2 norm of A. Default = 1.0E-6.
11-10	E	TOLR	Residual force norm convergence tolerance. Convergence is assumed, if $\left(\frac{\|\|R_j\|\|}{\|\|F_n\|\|}\right)^{1/2} \leq$ TOLR. where R is the residual load vector and F is the applied force vector. Default = 0.001.

Note: Convergence of the solution for a time step is assumed if either convergence tolerance is satisfied. It is recommended that the force tolerance condition be satisfied and the displacement tolerance be used to stop a nonconverging step.

IX. JAC Output Description

Printed output is produced by echoing the input for file FT05 and then writing a detailed description of each input card image.

A plot output file is written on FT11 by JAC and may be sent to the VAX for post processing with the BFTOV1 procedure. The following variables are written to the plot tape.

Nodal	Description
DISX or DISR	Total displacement in x or r-direction*
DISY or DISZ	Total displacement in y or z-direction*
RESX	Total residual force in x-direction
RESY	Total residual force in y-direction

Element	Description
SIGX or SIGR	Stress T_{xx} or T_{rr}
SIGY or SIGZ	Stress T_{yy} or T_{zz}
SIGZ or SIGT	Stress T_{zz} or T_{tt}
SIGXY or SIGRZ	Stress T_{xy} or T_{rz}
EPX1	Material history variables**
EPX2	
.	
.	
EPX10	
TEMP	Temperature at the center of the elements

Global	Description
RN	Residual force norm
RNN	Residual force tolerance
UN	Incremental displacement norm
UNN	Incremental displacement tolerance
FN	Applied force norm

RX or RR	Total reaction force in x or r-direction***
RY or RZ	Total reaction force in y or z-direction
NITER	Accumulative total number on iterations

* If a load step does not converge the incremental displacements of the nonconverged load step are written to FT11 and the printed output file.

** The values in the history variable arrays depend upon the material models used in the analysis. The number on arrays output to the plot tape is the maximum number needed by any material model. The following is a description of the variables by material type.

*** The reaction force in the R-direction has unit of force per radian.

Material Type 1 - Isothermal Elastic-Plastic

Name	Description
EPX1	Yield surface center stress component γ_{xx} or γ_{rr}
EPX2	Yield surface center stress component γ_{yy} or γ_{zz}
EPX3	Accumulated plastic strain
EPX4	Yield surface center stress component γ_{xy} or γ_{rz}

Material Type 2 - Temperature Dependent Elastic-Plastic

Name	Description
EPX1	Yield surface center stress component γ_{xx} or γ_{rr}
EPX2	Yield surface center stress component γ_{yy} or γ_{zz}
EPX3	Current yield stress
EPX4	Yield surface center stress component γ_{xy} or γ_{rz}

Material Type 3 - Temperature Dependent Secondary Creep

Name	Description
EPX1	Current effective creep strain

Material Type 4 - Isothermal Finite Strain Soil and Crushable Foam

Name	Description
EPX1	Current effective plastic strain
EPX2	Current volumetric strain

Distribution:

H. N. Abramson, Vice President
Enginnering Sciences
Southwest Research Institute
8500 Culebra Road
San Antonio, TX 78284

Los Alamos Scientific Laboratory (2)
P.O. Box 1663
Los Alamos, NM 87545
Attn: C. A. Anderson, Q-13, MC-576
J. J. Ruminer, WX-3, MC-931

Massachusetts Institute of Technology
Department of Mechanical Engineering
Cambridge, MA 02139
Attn: K. J. Bathe, Room 3-356

Northwestern University
Department of Engineering
Technological Institute
Evanston, IL 60201
Attn: T. Belytschko

Cities Service Company
Energy Resources Group
Exploration & Production Research
P.O. Box 3908
Tulsa, OK 74102
Attn: W. R. Jamison

Pacifica Technology
P.O. Box 148
Del Mar, CA 92014
Attn: R. S. Dunham

University of Washington
Mechanical Engineering Department
Seattle, WA 98105
Attn: A. Emery

University of Arizona
Tucson, AZ 85721
Attn: R. H. Gallagher
Dean of Engineering

Professor Michel Geradin
Laboratoire D'Aeronautiques
et Spatiales
Rue du Val Benoit, 75
Universite de Liege
B-4000 Liege
BELGIQUE

University of California
Lawrence Livermore Laboratory
P.O. Box 808
Livermore, CA 94550
Attn: G. L. Groudreau, L-122
J. O. Hallquist, L-122

Structural Mechanics
Reactor Technology
Westinghouse Advanced Reactors Division
P.O. Box 158
Madison, PA 15663
Attn: D. S. Griffin, Manager

Knolls Atomic Power Laboratory
P.O. Box 1072
Schenectady, NY 12301
Attn: F. Janucik

University of New Mexico
Department of Civil Engineering
Albuquerque, NM 87131
Attn: R. Johnson

Brigham Young University
Civil Engineering Department
Provo, UT 84602
Attn: S. E. Benzley

Argonne National Laboratory
Reactor Analysis and Safety Division
9700 South Cass Avenue
Argonne, IL 60439
Attn: J. M. Kennedy

Stanford University
Division of Applied Mechanics
Department of Mechanical Engineering
School of Engineering
Stanford, CA 94305
Attn: T. J. R. Hughes

University of California
Division of Structural Engineering and
Structural Mechanics
Department of Civil Engineering
Berkeley, CA 94720
Attn: R. Taylor, Rm 705, Davis Hall

Massachusetts Institute of Technology
Aeroelastic and Structures Research
Laboratory
Department of Aeronauatics & Astronautics
Cambridge, MA 02139
Attn: E. A. Witmer, Director

GWU-NASA Langley Research Center
Hampton, VA 23665
Attn: A. R. Noor, MS 246

University of Texas at Austin
Department of Aerospace Engineering
and Engineering Mechanics
Austin, TX 78712
Attn: J. T. Oden
E. B. Becker

Internal Distribution:

0313 J. T. Schamaun
1510 J. W. Nunziato
1511 D. K. Gartling
1511 R. R. Eaton
1511 D. F. McTigue
1520 D. J. McCloskey
1521 R. D. Krieg
1522 R. C. Reuter
1523 J. H. Biffle (60)
1524 W. N. Sullivan
1530 L. W. Davison
1531 B. J. Thorne
1531 T. Canfield
1533 W. T. Brown
1533 W. R. Davey
1533 M. E. Kipp
1533 S. T. Montgomery
1533 J. W. Swegle
1534 D. S. Drumheller
1534 T. G. Trucano
1540 W. C. Luth
1541 J. B. Rundle
1542 B. M. Butcher
1542 W. W. Wawersik
1642 L. F. Shampine
1814 T. R. Guess
2321 P. J. McDaniel
2646 M. R. Scott
5162 S. D. Meyer
6247 R. E. Glass
6310 T. O. Hunter
Attn: L. W. Scully, 6311
J. R. Tillerson, 6313
6313 M. E. Ford
6322 J. Wellman
6323 H. R. Yoshimura
6330 L. D. Tyler
Attn: D. E. Munson
6442 W. A. Von Riesemann
6442 T. E. Blejwas
6444 S. L. Thompson
6444 J. M. McGlaun
8120 L. D. Bertholf
8121 G. A. Benedetti
8121 M. L. Chiesa
8121 J. C. Keilman
8121 L. E. Voelker
8122 M. L. Callabresi
8122 J. E. Grant
8122 W. E. Mason, Jr.
8122 L. M. Napolitano
8122 L. I. Weingarten
8123 M. R. Birnbaum
8123 D. J. Bammann
8123 N. D. Gilbertsen
3141 C. M. Ostranter (5)
3151 W. L. Garner (3)
3154-2 C. H. Dalin (25)
(Unlimited Release for
DOE/TIC)
8424 M. A. Pound